MAGNETIC RESONANCE IMAGING OF PROXIMAL FEMUR AND SURROUNDING MUSCLES: *IN VIVO* PRECISION

A Thesis Submitted to the College of

Graduate Studies and Research

In Partial Fulfillment of the Requirement

For the Degree of Biomedical Engineering

University of Saskatchewan

Saskatoon

By

Leina Liao

PERMISSION TO USE

In presenting this thesis/dissertation in partial fulfillment of the requirement for a postgraduate degree from the University of Saskatchewan, I agree that the Libraries of this University may make it freely available for inspection. I further agree that permission for copying of this thesis/dissertation in any manner, in whole or in part, for scholarly purposes may be granted by the professor or professors who supervised my thesis/dissertation work or, in their absence, by the Head of the Department of the Dean of the College in which my thesis work was done. It is understood that any copying or publication or use of this thesis/dissertation or parts thereof for financial gain shall not be allowed without my written permission. It is also understood that due recognition shall be given to me and to the University of Saskatchewan in any scholarly use which may be made of any material in my thesis/dissertation.

DISCLAIMER

Reference in this thesis/dissertation to any specific commercial products, process, or service by trade name, trademark, manufacturer, or otherwise, does not constitute or imply its endorsement, recommendation, or favoring by the University of Saskatchewan. The views and opinions of the author expressed herein do not state or reflect those of the University of Saskatchewan, and shall not be used for advertising or product endorsement purposes.

Requests for permission to copy or to make other uses of materials in this thesis/dissertation in whole or part should be addressed to:

Head of the Division of Biomedical Engineering

University of Saskatchewan

Saskatoon, Saskatchewan S7N 5A9

Canada

ABSTRACT

Background: Hip fractures are a major health problem in Canada, and two main contributors to hip fracture are weak bone strength and fall. Weak muscles also negatively affect bone strength and increase the likelihood of falling. Advanced imaging techniques, such as magnetic resonance imaging (MRI), offer *in vivo* measurement of bone strength and muscle area at the proximal femur. However, it is not known if MRI-based measurements of bone and muscle properties are repeatable (i.e. precise).

Methods: The femoral neck and shaft of 14 healthy participants were scanned three times, using a 1.5T MRI with repositioning between scans. Boundaries of the femoral neck, shaft and four muscle groups were delineated semi-automatically. Geometrical and strength properties of bone and area of muscle groups were determined based on segmented images. The short-term precision errors (root mean square coefficient of variation; CV_{rms}%) between the repeated measures were calculated accordingly.

Results: MRI-based measures of bone geometry and strength and muscle area at the proximal femur demonstrated *in vivo* precision errors < 7.6%. The average CV_{rms}% for bone measures and muscle area were less than 4% and 2.5% respectively. Higher CV_{rms}% (e.g. average: 4.8%) was obtained for bone strength properties.

Conclusion: This is the first study to evaluate the *in vivo* performance of MRI on application to the proximal femur and surrounding muscles. Results demonstrate that MRI is a promising non-ionizing technique that offers precise measures of bone and muscle at the proximal femur.

ACKNOWLEDGEMENTS

Foremost, I would like to express my sincere gratitude to my supervisors Prof. James D. Johnston and Prof. Saija Kontulainen for their continuous support during my M.Sc. study and research, for their patience, motivation, enthusiasm, and immense knowledge. Without their guidance and persistent help this dissertation would not have been possible. Also, their positive academic attitude encouraged me to stay positive in my future study or career life.

I would like to thank my committee members, Prof. Allan T. Dolovich, Prof. David Leswick and my external examiner Prof. Haron Obaid, for their encouragement and insightful comments.

I would like to thank all volunteers who participated in this study. I appreciate Andrew Frank for assistance in participant recruitment and Jennifer Layton for skillful MRI measurements.

I would like to acknowledge the Canadian Institutes of Health Research (CIHR) for funding this study.

My appreciation goes to many mentors from many backgrounds: Prof. Dean Chapman, Prof. David Cooper, Prof. Jon Farthing and Prof. Gordon Sarty.

My sincere thanks also go to my fellows from our research group: Dena Burnett, Jackie Wang, Majid Nazemi, Morteza Amini, Madison Adam and Unyime Umoh, for creating this enjoyable working environment.

Last but not the least, thanks to my family includes my parents Chun Liao and Yunfeng Wang, for their endless love and support throughout my life; my grandparents Hengshan Wang and Jie Zhang, for their heartwarming; also my uncle Weifeng Wang, for being my spiritual mentor.

TABLE OF CONTENTS

LIST OF TABLES

LIST OF FIGURES

LIST OF ABBREVIATIONS

Abbreviation	Description
2D	Two-dimensional
3D	Three-dimensional
aBMD	2D areal apparent bone mineral density (g/cm^2); DXA measure
BMC	Bone mineral content (mg or g)
BMD	Bone mineral density (g/cm^2 or g/cm^3)
BR	Buckling ratio
CT	Computed tomography
CV%	Percentage coefficient of variation
DOF	Degree(s) of freedom
DXA	Dual-energy X-ray absorptiometry
HMH	Half-maximum height
HSA	Hip Structural Analysis
HU	Hounsfield unit
ICC	Intraclass correlation coefficient
MRI	Magnetic resonance imaging
QCT	Quantitative computed tomography
RMS	Root mean square
ROI	Region of interest
SD	Standard deviation
WHO	World Health Organization

GLOSSARY

Term	Definition
Anterior	Front plane of a body; referring to surface facing forward
Areal bone mineral density	Imaging measure of bone mineral content/image area (g/cm^2) as measured by DXA
Axial	Plane that divides the body into superior and inferior parts
Bone marrow	The fatty network of connective tissue that fills the cavities of bones, also containing red blood cells
Bone mineral density	Imaging measure of bone mass/total image area
Coronal	Plane that divides the body into anterior and posterior sections
Cortical bone	Type of bone tissue comprises of multiple layers of compacted bone; forms the cortex or outer shell of bone; much denser, stronger and stiffer than trabecular bone
Endosteal boundary	A boundary between inner surface of cortical bone and trabecular bone or bone marrow, referring to the inner layer of cortical bone
In vivo	Latin for "within the living", experimentation using a whole, living organism as opposed to partial or dead organism
Inferior	Bottom location of a body; referring to the bottom surface or region
Lateral	Situated at or extending to the side
Medial	Situated at or extending to the middle
Musculoskeletal	Denoting the musculature and skeleton together
Periosteal boundary	A dense fibrous layer covers the surface of bones (except at the long bone ends), referring to the outer fibrous layer of cortical bone
Pixel	A tiny area of illumination on a display screen; thousands of them compose a full image

Proximal	Pertains to different ends of an extremity; proximal end of extremity is the end situated nearest the center of the body (e.g. proximal femur is located at pelvic region)
Sagittal	Plane that travels from the top to the bottom of the body, dividing it into left and right portions
Trabeculae	Latin for “small beam”; bone tissue element in the form of a small beam, strut or rod
Trabecular bone	Type of bone tissue referring to bone with vertical or horizontal trabeculae, forms a spongy like structure; less dense than cortical bone

LIST OF SYMBOLS

Symbols	Definition
A	Area
c	Distance
I_{max}	Principal moment of inertia; maximum bending resistance
I_{min}	Principal moment of inertia; minimum bending resistance
I_x	Area moment of inertia relative to x axis
I_y	Area moment of inertia relative to y axis
I_{xy}	Product moment of inertia
M	Moment
R	Radius to the periosteal surface
r	Radius to the endosteal surface
t	Cortical thickness
Z_{max}	Section modulus; maximum bending resistance
Z_{min}	Section modulus; minimum bending resistance
Z_p	Torsional rigidity; stiffness of bone to resist applied torque
φ	Angle
σ	Stress

1 INTRODUCTION

1.1 Overview

Hip fractures are a major health problem and economic burden in Canada [1]. Hip fracture may consequently lead to a patient's disability and mortality [2]. A tool capable of identifying fracture-prone individuals may help alleviate the burdens of hip fractures.

Bone strength, or the ability of bone to withstand an applied stress without fracture [3], is regarded as the indication of bone condition and susceptibility to fracture. Bone strength is related to bone geometry and material properties [3]. Information regarding the strength of the hip (proximal femur) and surrounding muscle is invaluable and may help reduce risk of falling-related injuries, such as fractures. In addition, bone strength is influenced by forces exerted by surrounding muscles (i.e. muscle-bone interactions) [4]. Evidence indicates that muscle affects bone adaptation on its mass, structure and strength [5]. Importantly, falling is another strong risk factor for fracture and weakened muscle increases risk of falling [6-8]. Currently researchers are seeking a precise and safe technique to measure bone and muscle properties.

The use of advanced imaging techniques has become a mean to estimate bone strength and measuring muscle *in vivo*. However, current imaging techniques for such purposes are limited. Dual-energy X-ray absorptiometry (DXA) is limited to 2D images, and does not provide 3D structural information about bone and muscle. Although DXA-based Hip Structural Analysis (HSA) provides estimates of bone geometry and strength, it provides little information about muscle structure and is limited to 2D projectional images. Computed tomography (CT) offers precise 3D representations of musculoskeletal structure, but at the expense of high radiation dose

which could be harmful to a participant's health [9]. One imaging technique offering potential to provide 3D measures of hip geometry and strength is magnetic resonance imaging (MRI). In addition, the superior soft tissue contrast of MRI makes imaging of muscle area feasible [10]. Of note, in the biomedical field, muscle area is often used as a surrogate estimate of muscle force [11]. However, the precision of MRI (or the ability to present repeatable results) in bone strength estimation and muscle area measurement at the proximal femur is currently under-explored.

The specific objective of my research was to assess the *in vivo* precision of MRI-based measures of bone strength and geometry at the hip femoral neck and shaft, in addition to muscle size (area). Through this study, the potential utility of MRI for assessing bone and muscle properties is evaluated.

1.2 Scope

Chapter 2 provides an overview of hip anatomy, including proximal femur and surrounding muscles; a brief review of hip fracture, such as severity, risk factors, characterization, pathogenesis and current assessment methods for fragile bone; relations between femur strength/surrounding muscle area and hip fractures; and fundamental mathematical equations for estimating bone strength. Chapter 3 presents research questions and study objectives. Chapter 4 outlines the methodological details of the *in vivo* short-term MRI precision study. Chapter 5 presents precision results from this study. Chapter 6 discusses study results, including a comparison of study results to previously reported results, and strengths and limitations of this study. Chapter 7 concludes this study, outlines significance, and offers recommendations for future studies.

2 LITERATURE REVIEW

2.1 Functional Anatomy

2.1.1 Hip Joint

The hip joint is a classical ball-and-socket structure, where the ball refers to femoral head (which is convex) and the socket refers to the acetabulum (which is concave) [12] (Figure 2-1). The head of the femur fits into the acetabulum and articulates within it, thereby forming the hip joint. The acetabulum is coated with cartilage around most of its periphery except the central and inferior compartments, which form a horseshoe-shaped structure [13]. At the central inferior acetabular fossa, it contains a synovial covered fat pad which provides shock absorption and reduced friction between surfaces [12]. Labrum, a fibrocartilaginous tissue, attaches to the rim of the acetabulum. It plays a role in enhancing the mechanical stability of the hip joint and also preventing synovial fluid from leaking to the peripheral compartments of the hip joint [12, 14]. The stability of the hip joint is “secured” by the hip capsule (capsular ligament), which also ensures the hip joint functions properly and prevents from dislocation [14].

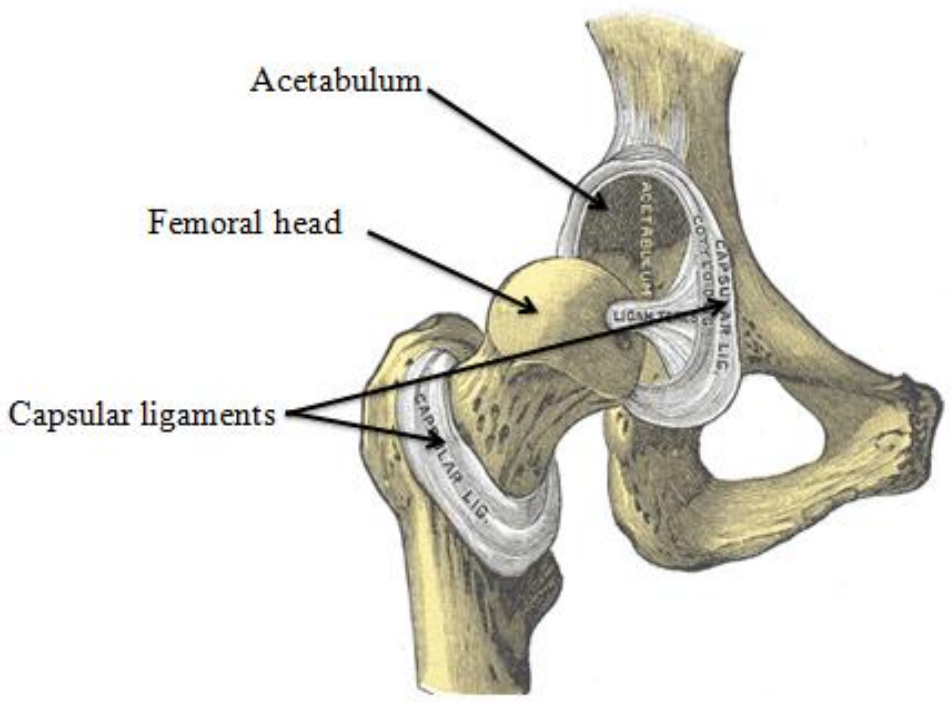

Figure 2-1. Anatomy of hip joint, including the femoral head, acetabulum and capsular ligaments. Modified from Gray's Anatomy [15].

The hip is loaded differently in circumstances of two-leg stance (e.g. standing) and one-leg stance (e.g. walking, running or other out-of-plane activities). At the hip joint, the load (e.g. body weight) is transferred to the acetabulum and then to the femoral head through contact area. In the circumstance of standing, or two-leg stance, the whole body weight minus the weight of both legs is loading equally on both femoral heads with the center of gravity located at the center of both hip joints [12]. In contrast, the loading condition changes in the circumstance of other one-leg postures and activities, or one-leg stance. The center of gravity shifts laterally and away from the supporting lower limb because of the inclusion of the weight of the non-supporting lower limb [12] (Figure 2-2). Also taking the forces exerted by surrounding muscles into account, the supporting lower limb bears a higher load in one-leg stance than in two-leg stance.

Importantly, hip fracture occurs at the proximal femur because of larger force transmitted than the bone can bear, which causes bending and compression of the bone.

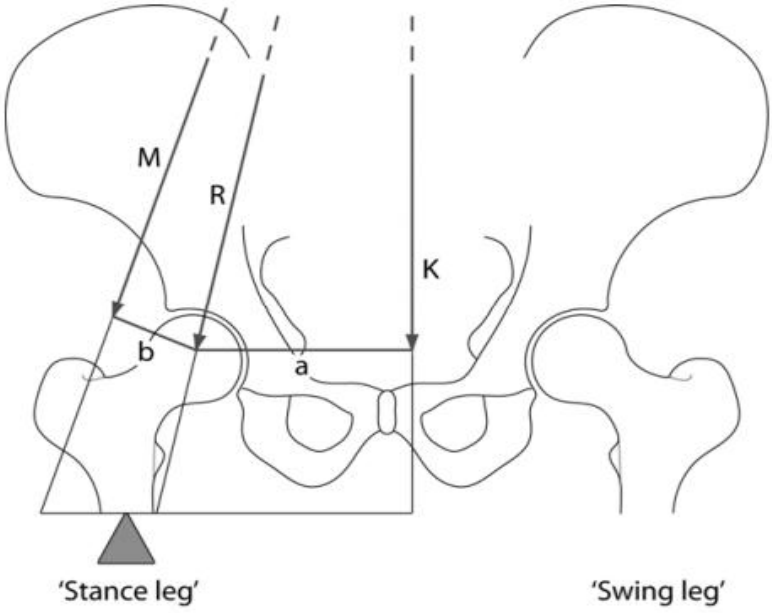

Figure 2-2. A diagram illustrates hip joint force in the circumstance of walking (i.e. one-leg stance), where K is the weight of body minus the weight of the supporting lower limb (i.e. stance leg), M is the force exerted by muscle, R is the joint reaction force, a is the moment arm of K, and b is the moment arm of M [12].

2.1.2 Proximal Femur

The proximal femur anatomically consists of the femoral head, neck, trochanter and shaft (Figure 2-3). The femoral head is a globular structure coated with cartilage on its smooth surface that lubricates the joint movement. The femoral neck extends from the femoral head and then meets trochanteric region, which includes the greater trochanter and the lesser trochanter. The femoral neck is the narrowest cross-section of the entire femur (i.e. most susceptible to hip fracture),

which bears compression and bending in the majority of circumstances [16-17]. Ligamentous and muscular forces generate compressive stress, while bipedalism (i.e. motions such as walking) produces bending stress at the femoral neck [16-17]. The compressive loads are transmitted to the femoral shaft, the tubular-shaped structure located immediately below the lesser trochanter, which makes the femoral shaft mostly experience compression rather than bending [17-18]. In the case of fall, the shaft is mostly subjected to bending which leads to high-energy fracture (i.e. a type of fracture which commonly happens to young and healthy bone by incidences such as car accident and height falling [19]).

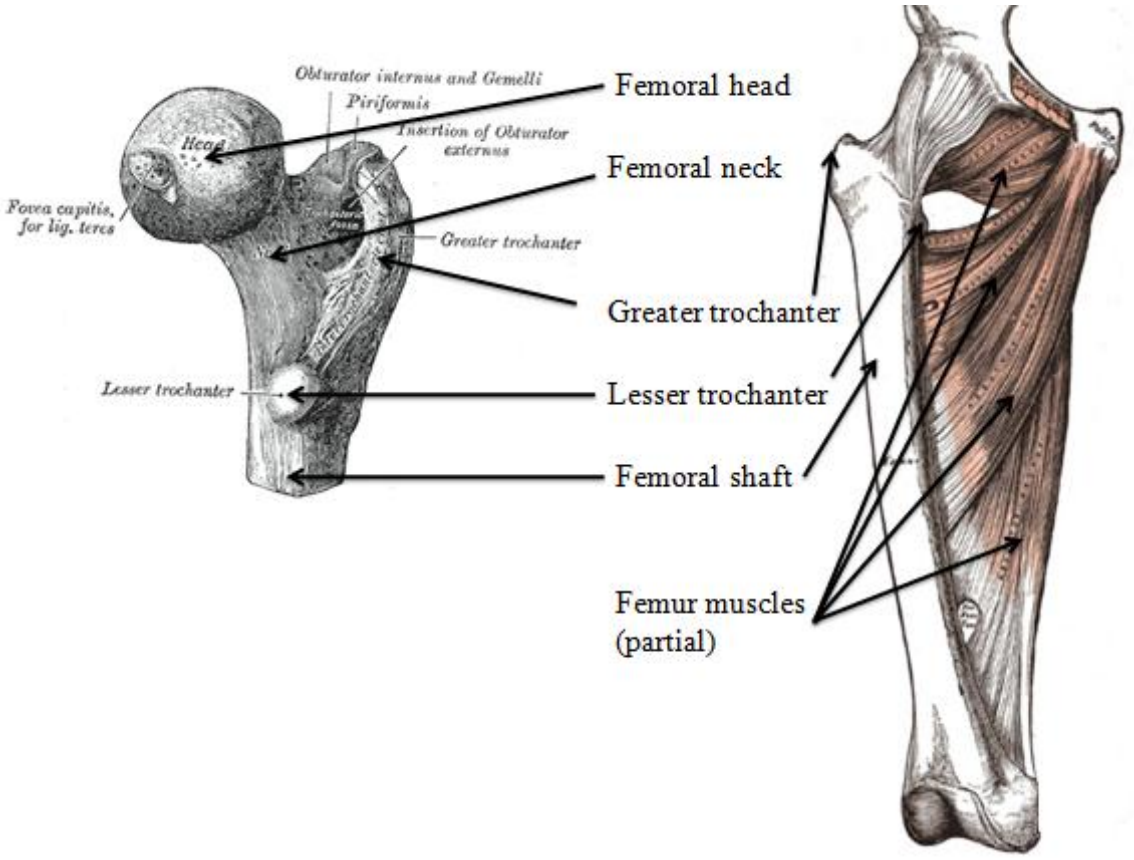

Figure 2-3. An illustration of the proximal femur (left) and anterior view (right) of the overall femur and part of femur muscles, showing the locations of the femoral head, neck, shaft, greater trochanter and lesser trochanter. Modified from Gray's Anatomy [15].

From a macroscopic point of view, the femur consists of cortical and trabecular bone, and is partially infiltrated with bone marrow (Figure 2-4). Cortical bone, or compact bone, forms a dense outer layer called the cortex to provide major support to the whole body. Cortical bone loss, or cortical thinning, occurs with aging which increases bone fragility [9, 20-22]. Trabecular bone, or cancellous bone, is a more porous bone enclosed by the cortical bone. At the femoral shaft, instead of trabecular bone, bone marrow exists in the cortical shaft and there is little to no trabecular bone. Bone marrow has two types: red and yellow bone marrow. Red bone marrow consists mainly of hematopoietic tissue, which produces blood cells in mammals; while, yellow bone marrow is mainly composed of fat cells. In the elderly, more yellow bone marrow is generated rather than red bone marrow [9].

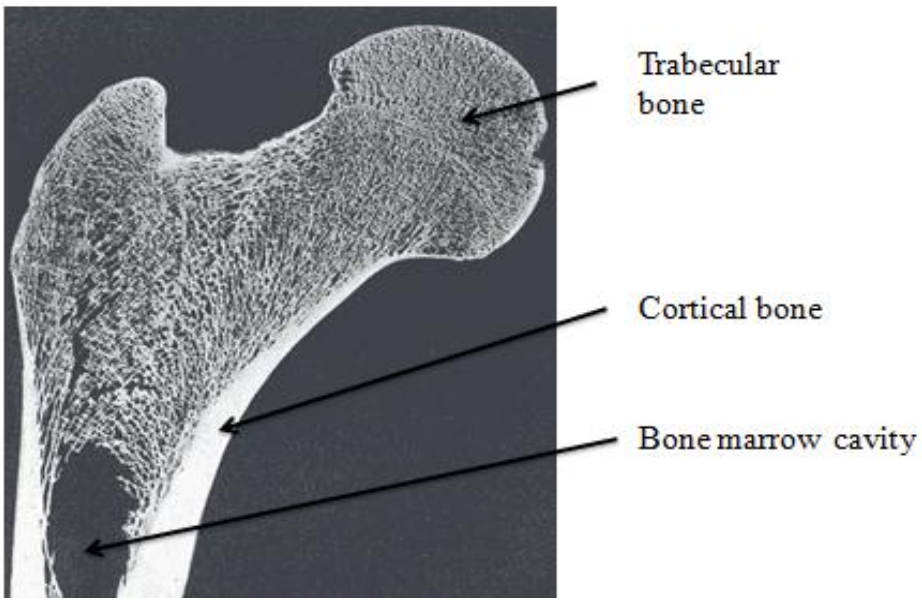

Figure 2-4. Internal structure of the proximal femur, showing that the femoral neck contains trabeculae surrounded by a layer of thin cortical bone. However, the femoral shaft contains a marrow cavity which is surrounded by a thick cortical layer. Modified from Gray's Anatomy [15].

2.1.3 Surrounding Muscles of Proximal Femur

There are numerous muscles at the hip region and along the femur which help produce movement and maintain balance of the human body. Femur muscles, such as extensors, adductors, abductors and flexors, are naturally built for different purposes. Extensors plays an important role in extending the femur from the lumbo-pelvic complex, e.g. pull the knee down and backward; adductors provide medial movement of the lower limb towards the middle of the body, e.g. moving the femur inward with hip straight; abductors are responsible for lateral movement away from the midline of the body, e.g. moving the lower limb outward to the side; flexors acts for flexing the femur onto the lumbo-pelvic complex, e.g. pull the knee upward. Muscles attach to bone through tendon (i.e. a fibrous connective tissue) and exert forces on bone which influences the resistance of the bone to fracture [23].

2.2 Hip Fractures

Hip fractures are a major health problem and economic burden in Canada [1]. Hip fractures affect approximately 30,000 people each year in Canada [24-25]. Severe hip fracture can consequently lead to a patient's disability and mortality [2]. In 1996-1997, the annual cost to care for hip fracture patients to the Canadian Health Care System was estimated at 650 million dollars. This amount is expected to rise to 2.4 billion annually by 2041[24].

2.2.1 Risk Factors

Risk factors for hip fracture have been determined in several studies [26-29], including weakened bone and muscle strength, falling risk and individual clinical characteristics [30]. Bone strength, or the ability of bone to withstand an applied stress without fracture [3], is regarded as an indication of bone's health condition. Osteoporosis, a bone disease characterized by compromised bone strength [3], is commonly linked to low-energy fracture [19, 31-33] (i.e. a type of fracture which commonly happens to weakened bone by incidences such as fall to the side [19]), with 70-90% of hip fractures being linked to osteoporosis [25]. In addition to weak bone strength, numerous studies show that falling is another strong risk factor for hip fracture [6-8]. More than 95% of hip fractures result from a fall [30]. Among people with hip fracture, approximately 90% are elderly people [34]. Studies reveal that people are more likely to experience fall if they have weakened muscles, or have lower muscle force [35-36]. It is widely recognized that muscle area is a surrogate measure of muscle force and is positively related to each other [5]. Muscles provide adequate muscle force to balance the body and prevent accidental falls, but diminish in area at older stages. This increases fall risk, unless external training to maintain muscle area is conducted continuously. Moreover, individual clinical characteristics have also been found to affect the risk of hip fracture, such as physical activity levels, estrogen exposure, fracture history, calcium and vitamin D intake, cigarette smoking and alcohol use. [30].

2.2.2 Characterizations and Pathogenesis

Compared with healthy bone, the fragile femur shows alternations in its morphology and mechanical properties. Morphologically, a femur with thinner cortical thickness is more

susceptive to fracture [37-38]; the same for the femur surrounded by smaller muscles [35-36]. This is due to bone and muscle experiencing gradual loss with aging. As age increases, more resorption of bone cells happens rather than formation. This increases endosteal bone resorption and reduces periosteal bone formation [39-40]. Changes in morphology of bone compromise its resistance to fracture [19, 33, 41-42]. Dickenson et al. found that the mechanical properties of fragile bone (e.g. osteoporotic bone), such as strength and stiffness, are less than that of normal bone [41]. He also found that fragile bone shows reduced ability to absorb energy before fracture than normal bone; however, this is not linked to changes in mineral content (e.g. bone mineral mass or density) [41]. Later, Chen et al. found that the changes in morphology, such as the age-related thinning effect of the cortical bone, compromise the capacity of the whole structure to absorb energy [42].

2.2.3 Current Assessment Methods

Advanced imaging techniques are used to define whether bone is prone to fracture through measuring bone mineral density (BMD; a measure of bone quality), bone geometry and strength [43]. The World Health Organization (WHO) proposed a scoring system (i.e. T score) to evaluate bone fragility, according to the standard deviation (SD) of patient's BMD value to a reference population (i.e. healthy individuals, 30 years of age, same sex, who have peak bone mass). For instance, the bone is defined as normal if $-1 \leq$ T score $\leq +1$; the bone is defined to be less strong than the normal bone if $-2.5 <$ T score < -1 (i.e. osteopenia); the bone is defined to be more fragile or one or more fragility fractures have already presented if T score ≤ -2.5 (i.e. osteoporosis) [44]. However, this assessment method is queried by many studies because a substantial amount of hip fractures happen to individuals who were previously diagnosed as

having normal bone [45-48]. For example, in a population study of 5794 participants, only ~2/5 women and ~1/5 men who experience non-vertebral fractures were previously classified as having fragile bone [46]. It is suggested that assessment of bone geometry and strength should be taken into account for evaluation of bone's condition [9]. Non-invasive imaging techniques are applied, *in vivo*, to characterize bone geometry and derive estimates of bone strength based upon its geometrical properties. Some of those imaging techniques can also be employed to assess muscle area [5].

2.3 Hip Fracture and Femur Bone Strength

Fractures occur increasingly at the femoral neck and shaft [9, 49-50]; therefore, more attention has been paid to these sites to reduce the risk of hip fracture. At the proximal femur, the femoral neck is apparently regarded as the weakest site due to a small area and thin cortical thickness [9]. Theoretically, the femur can withstand an applied stress if the stress is less than the bone strength of the femoral neck. Thereby, the neck has claimed to be the most crucial site for characterizing the overall proximal femoral strength [9]. With aging, cortical thickness diminishes at both femoral neck and shaft sites, leading to fracture susceptibility at both sites [51]. Further, there have been recent heightened incidences of femoral shaft fracture, perhaps due to medication usage for reducing bone loss [49-50]. Therefore, it is important to estimate the bone strength at these two sites through reliable measurement.

Studies reveal that bone strength is determined by bone geometry in addition to BMD [3, 9, 45-46, 52]. Importantly, BMD can only partially explain the bone strength, which can give rise to inaccurate indications of susceptibility to hip fracture if diagnosis is based solely on BMD.

Several studies have demonstrated that bone strength is strongly affected by changes in bone geometry [53-56]. In the field of engineering, when a beam is loaded in bending, the stress can be expressed by

$$\sigma = \frac{Mc}{I} \tag{2-1}$$

where σ denotes the bending stress; c denotes the distance from the neutral axis; M denotes the bending moment; and I refers to the area moment of inertia.

For a given value of M, bending stress can be reduced by either decreasing c or increasing I. I is a strength index of a structure, which is related to the geometrical properties of the structure. For example, for a tubular bone, the area moment of inertia (I) is given by

$$I = \frac{\pi}{4}(R^4 - r^4) \tag{2-2}$$

where R refers to the periosteal radius and r refers to the endosteal radius. For reference, R approximately equals to 1.8 times r for mammalian long bones [57], which makes $I=0.71R^4$.

Thus, an increase of 10% in R will result an increase of 46% in I. As age increases, R and r may expand differently as a result of bone formation on the periosteal surface and bone resorption on the endosteal surface. For instance, R increases by 10% while r increases by 35%, resulting in a decrease of 6% in the cortical area, which still causes I to increase 27% [58] (Figure 2-5). This explains the phenomenon that although cortex thinning happens, the bone strength may still remain the same if the bone diameter increases [59]. Therefore, deterioration in bone geometry increases the risk of hip fractures [53, 60-61].

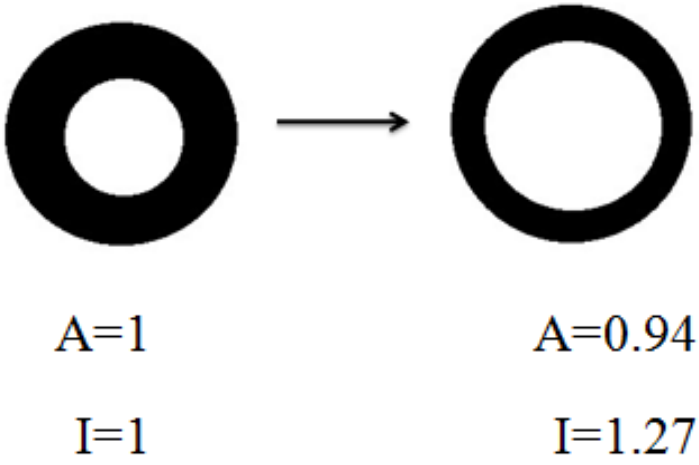

Figure 2-5. The structures represent the cross sections of tubular bone. The effect of aging is simulated by increasing the periosteal radius by 10% (i.e. bone formation on the periosteal surface) and the endosteal radius by 35% (i.e. bone resorption on the endosteal surface). This results in a decrease of 6% in the cortical area, however, an increase of 27% in the area moment of inertia I. It demonstrates that I is related to the geometrical properties of the structure, such as radius or diameter of a tubular structure. Modified from [58].

Imaging-based bone geometrical and strength properties are strongly associated with failure load measured through mechanical testing [62]. Mechanical testing on the bone is the "gold standard" for determining bone's mechanical properties, such as the bone strength. The failure load can be measured through mechanical testing, which refers to the load that causes failure of a material (e.g. bone fracture). A previous study reported the relationships between imaging-based bone variables and mechanical testing-based failure load [62]. At the femoral neck, magnetic resonance imaging (MRI)-derived cortical area and area moment of inertia had high associations with the failure load, explaining 46% and 48% of the total variance (r^2), respectively [62]. This study reveals that as a non-invasive approach, imaging techniques such as

MRI are able to provide compatible estimations of bone geometry and strength to mechanical testing-based measures.

2.4 Bone Strength Indices

Principal moment of inertia (I_{max} and I_{min}), section modulus (Z_{max} and Z_{min}), torsional rigidity (Z_p) and buckling ratio (BR) are indices of bone strength, which can be derived from bone geometrical properties.

2.4.1 Area Moment of Inertia

Inertia aims to resist an object to a change to its current state, and area moment of inertia (I) refers to the resistance of an object to bending [63]. I is useful as an indication of bone strength under bending. A high value of I indicates large bone strength to resist bending. For a non-symmetrical tubular cross section (e.g. bone) in bending, a reference coordinate system m-n passes through its centroid. I_m and I_n refer to the bending resistance about the m and n directions, and are derived with respect to m-n axes. The equations for calculating I_m and I_n are [63]

$$I_m = \int n^2 dA \tag{2-3a}$$

$$I_n = \int m^2 dA \tag{2-3b}$$

where dA denotes the cross sectional area of a small area (e.g. a pixel); n denotes the distance from the centroid of the small area to the m axis; and m denotes the distance from the centroid of the small area to the n axis.

The parallel axis theorem is applied to find the I_m and I_n about any axes (m-n axes) that parallel to the reference x-y axes. Following equations are used [63]

$$I_x = I_m + Ay^2 \tag{2-4a}$$

$$I_y = I_n + Ax^2 \tag{2-4b}$$

where I_m and I_n refer to the area moment of inertia with respect to the reference m-n axes; I_x and I_y refer to the area moment of inertia about x-y axes parallel to m-n axes; A refers to the area of the object; and x and y refer to the distances from the centroid of the object to the x-y axes, respectively.

Product moment of inertia (I_{xy}), represents the "imbalance" of this cross section (e.g. rotation), is also derived with respect to x-y axes. The equation for calculating I_{xy} is [63]

$$I_{xy} = \int xydA \tag{2-5}$$

where x, y and dA are the same as those in equation 2-3.

Another coordinate system x'-y' exists at an angle to x-y axes is called principal axes, on which I_{xy} vanishes and the cross section is balanced (i.e. no rotation) (Figure 2-6). I_x and I_y calculated with respect to the principal axes are their maxima (I_{max}) and minima (I_{min}). I_{max} and I_{min} are the principal moments of inertia and represent the maximum and minimum bending resistance of an object, respectively. It is used for determining the locations of the strongest and weakest strengths of a cross section, respectively. The equations for calculating I_{max} and I_{min} are shown below [63]

$$I_{max} = \frac{1}{2}(I_x + I_y) + \frac{1}{2}(I_x - I_y)\cos 2\varphi - I_{xy}\sin 2\varphi \quad (2\text{-}6a)$$

$$I_{min} = \frac{1}{2}(I_x + I_y) - \frac{1}{2}(I_x - I_y)\cos 2\varphi + I_{xy}\sin 2\varphi \quad (2\text{-}6b)$$

$$\varphi = -\frac{1}{2}\arctan\frac{2I_{xy}}{I_x - I_y} \quad (2\text{-}6c)$$

where I_x and I_y refer to the area moment of inertia with respect to x and y respectively; I_{xy} refers to the product moment of inertia; and φ refers to the angle between the reference x-y axes and the principal axes x'-y'.

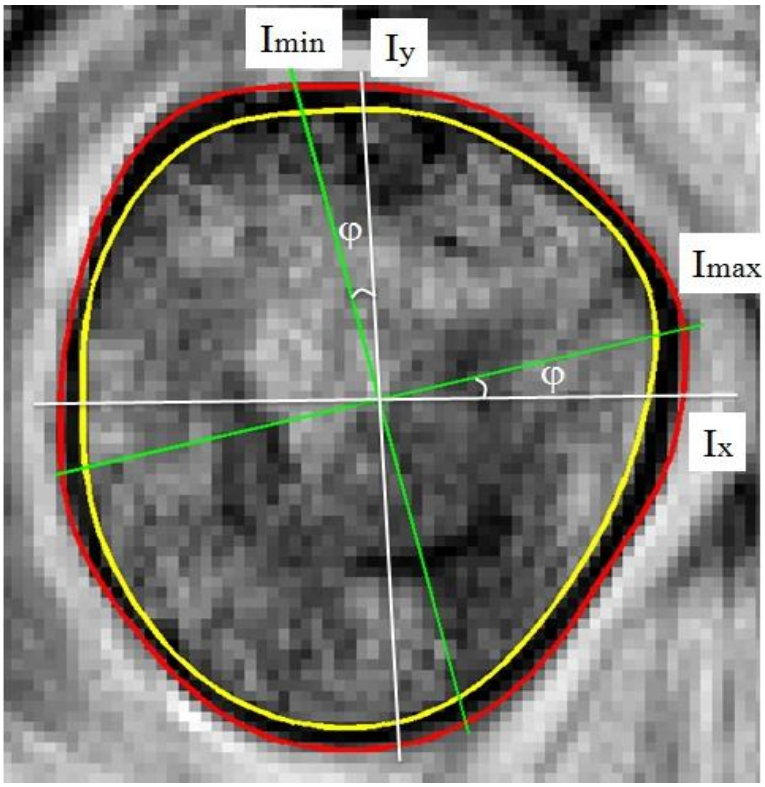

Figure 2-6 MRI image of the femoral neck. The neutral x-y axes are shown in white color, according to which I_x and I_y were calculated. The principal axes are shown in green color, on which I_{max} and I_{min} were calculated. On the principal axes, I_{xy} equals to 0. There is an angle φ between the two coordinate systems.

2.4.2 Section Modulus

Section modulus (Z) is also a bending strength index; a high value of Z indicates large bone strength to resist bending. The section modulus is better to describe the bone strength in comparisons between individuals [38]. Because each individual has different bone diameter, the farthest distance in the bone's cross section from the reference x-y axes varies. In calculating the section modulus, the variations in the shape of bone's cross section is disregarded, which makes the section modulus more suitable for comparison study. The equations for calculating Z_{max} and Z_{min} are shown below

$$Z_{max} = \frac{I_{max}}{(c_y)_{max}} \tag{2-7a}$$

$$Z_{min} = \frac{I_{min}}{(c_x)_{max}} \tag{2-7b}$$

Where $(c_y)_{max}$ and $(c_x)_{min}$ are the farthest distances from the reference x-y axes, respectively.

2.4.3 Torsional Rigidity

Torsional rigidity (Z_p) is another index of bone structural strength to determine the stiffness of bone to resist applied torque (i.e. torsional resistance). Z_p of any thin-walled cross section can be estimated using the classic Bredt's formula

$$Z_p = 2At \tag{2-8}$$

where A denotes the cross-sectional area enclosed by the median line of the periosteal and endosteal boundaries; and t denotes the thickness of the thin wall, such as cortical thickness.

2.4.4 Buckling Ratio

Buckling ratio (BR) is related to instability of bone. The bone can be induced to failure mode once it is subjected to buckling. For a bone in high compression, the critical stress (σ_{cr}) at which the bone becomes critically unstable (i.e. buckling) is [22]

$$\sigma_{cr} = 0.61\frac{t}{R} \times E \tag{2-9}$$

where t is the cortical thickness; R is the radius of bone; and E is the elastic modulus of the bone.

BR is essentially related to the ratio of t/R. The classic equation for calculating BR is [64]

$$BR = \frac{r_{max}}{t} \tag{2-10}$$

where r_{max} refers to the maximum distance from the outer boundary to the centroid (i.e. the maximum bone radius for a non-symmetrical structure); and t refers to the cortical thickness.

Another area-based approach to calculate BR is

$$BR = \frac{A_{tot}}{A_{cor}} \tag{2-11}$$

where A_{cor} is the area of cortical bone; and A_{tot} is the area of total bone. This approach is also related to the ratio of t/R.

2.5 Hip Fracture and Femur Muscle Area

Muscle forces impact bone strength and also prevent from falling [4-5, 35, 65-66]. Surrounding muscles affect femur bone strength through muscle-bone interactions [4]. The contractions of

regional muscles (i.e. resulting in force) induce natural stimuli for bone growth [4, 67]. Previous studies showed the existence of a close correlation between muscle area and bone strength [67-71]. Hogler et al. [67] conducted a study with 145 healthy subjects and reported a strong correlation between muscle area and cortical area of the proximal femoral shaft (r^2=0.91 for male and r^2=0.88 for female). It is also noted that bone loss is associated with a decrease in muscle mass and strength with aging [71-74]. In addition to weak bone strength, numerous studies showed that falling is another strong risk factor for fracture [6-8]. In the process of falling, the proper and adequate muscle strength plays an important role in decreasing fall risk [35-36].

Muscle area (i.e. a surrogate measure of muscle force) can be measured using imaging tools [5, 75-76]. Conventionally, muscle strength is measured by gripping a dynamometer [77]. The muscle strength, or the ability of muscle to generate forces, is linked to muscle area [78-79]. Currently, advanced imaging techniques are applied to provide *in vivo* information regarding muscle structure, including the muscle area [75-76].

2.6 Imaging Bone and Muscles

2.6.1 Dual-energy X-ray Absorptiometry (DXA)

Dual-energy X-ray absorptiometry (DXA) is a two-dimensional (2D) imaging tool which offers reliable assessments of BMD and body composition, but it is insufficient in describing the fragility of bone and overestimates muscle tissue [45-47, 80]. DXA uses x-ray at two energy levels passing through the body to derive regions of two different components, such as bone and soft tissue (e.g. muscle) in regions with bone. The principle of this technique is based on

differential attenuation by bone and soft tissue at two energy levels [81]. DXA image is thus constructed from a three-dimensional (3D) structure to a 2D projection. Using this principle, measures such as areal BMD (aBMD, g/cm^2) can be estimated, most commonly at the proximal femur and lumbar spine [82]. Even to date, the use of DXA is regarded as the gold standard for osteoporosis screening using scoring system defined by WHO [82]. However, a substantial number of bone fractures were found among the population who were previously diagnosed as non-osteoporotic [45-47]. This finding, again, reveals that bone strength is determined not only by BMD, but also varies with bone geometry [37-38]. On the other hand, because of the wide accessibility and being inexpensive to use, DXA becomes an alternative approach of body composition measurement. However, DXA was found to likely overestimate muscle tissue because of the inclusion of skin and other non-muscular tissue [80, 83].

DXA-based Hip Structural Analysis (HSA) is a method introduced to extract geometry and strength properties from DXA images beyond BMD, but is still associated with some technical and fundamental limitations [84]. The HSA method is based on the principle that a line of pixel values across the bone axis contain structure information about the corresponding cross section at this location, such as width and length [38, 85]. Then more geometrical properties, such as cross-sectional area, can be estimated based on certain assumptions and strength properties can be derived based on these structural and geometrical properties. Femoral neck (the narrowest cross section) and shaft (2 cm distal to the midpoint of the lesser trochanter) are measurable using this method [85]. Corresponding geometrical properties such as cortical thickness and strength properties such as cross-sectional moment of inertia, section modulus and buckling ratio can be estimated. However, those properties are calculated under an assumption of a circular annulus with percentage of material distribution assumed (Figure 2-7) [85-86].

Although HSA is capable of providing structural measurement, DXA scanner was originally designed for areal density measurement. Poor spatial resolution and 2D presence of image (e.g. limited geometrical information in one plane) complicate the detection of bone structure, especially of very small structures and changes [84].

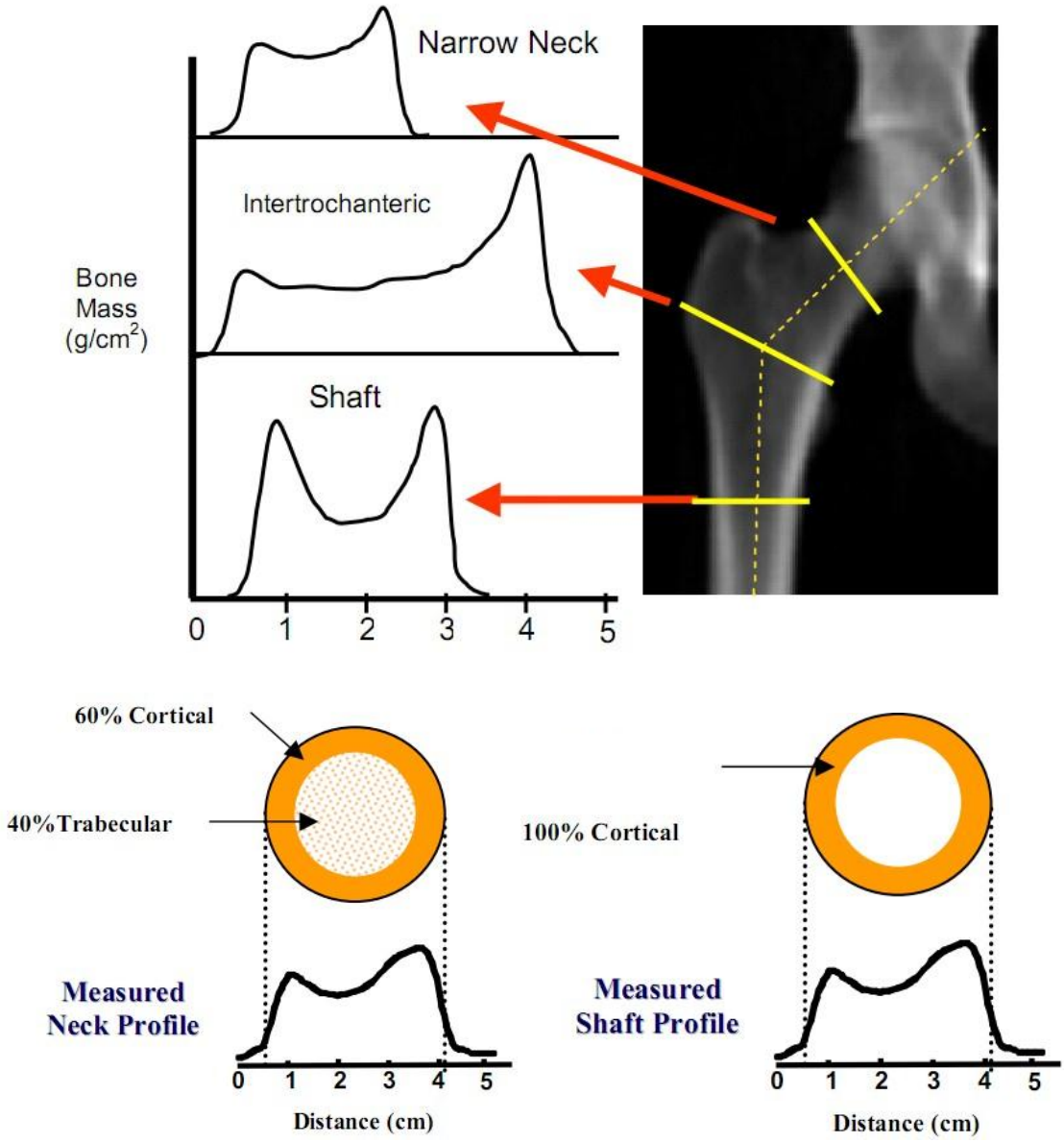

Figure 2-7 A DXA scan of hip (top), showing positions of analysis regions across the femur at the neck, intertrochanteric, shaft and corresponding typical bone mass profiles used in measurements of geometrical properties. In DXA-based HSA, an assumption of circular annuli is made with accounting 60/40 proportion of cortical/trabecular bone and 100% cortical bone in the neck (bottom left) and shaft (bottom right) regions, respectively [85].

2.6.2 Computed Tomography (CT)

Computed tomography (CT) is an X-ray based imaging technique that offers BMD and geometrical measurement of internal structures. CT possesses more advantages over DXA in most clinical imaging applications. CT images are generated by following two step processes: initial scan data acquisition and tomographic image (or thin imaged "slices" of measured structure) construction by applying mathematical calculations. Using a calibrated phantom, CT numbers that are measured in Hounsfield Units (HU) can be transformed into 3D volumetric BMD equivalents (mg/cm^3). 3D volume images of tissues can be reconstructed through aligning series of parallel images. The use of CT technique is increasing as it shows more advantages over DXA, such as 3D morphological measurement, rapid scanning time (current effective scan time: 80-200ms/slice) and capability of separate measures of cortical and trabecular bone [87-89].

To date, CT imaging is increasingly applied to investigate proximal femoral integrity, structure (Figure 2-8) and surrounding muscles (Figure 2-9) [48, 90-96]; but its use is limited to the low accessibility and radiation exposure issue. Jordan et al. conducted a retrospective study which revealed there is a vast increase in CT application for investigating occult hip fractures [92]. They found that, in 2006-2007, 20 CT scans were performed out of 547 hip fractured patients; however, this number of CT scans has increased to 239 out of 499 hip fractured patients in 2010-2011. The rapid increase in the use of CT is related to the reliable results it delivers. However, accessibility of CT is relatively low because of high cost and maintenance fees, compared to the use of DXA. Also, CT delivers a considerable dose of radiation to subjects depending on measuring location [97]. As for a 3D hip quantitative CT examination (15 cm scan length), an effective radiation dosage of 2.5-3 mSv is applied [98-99], which is much higher than the effective dosage of 0.009 mSv that a DXA scan delivers [100]. This compares with the annual

effective dose of 1.8 mSv from natural background in Canada [101] and 0.05 mSv during a transatlantic flight [102].

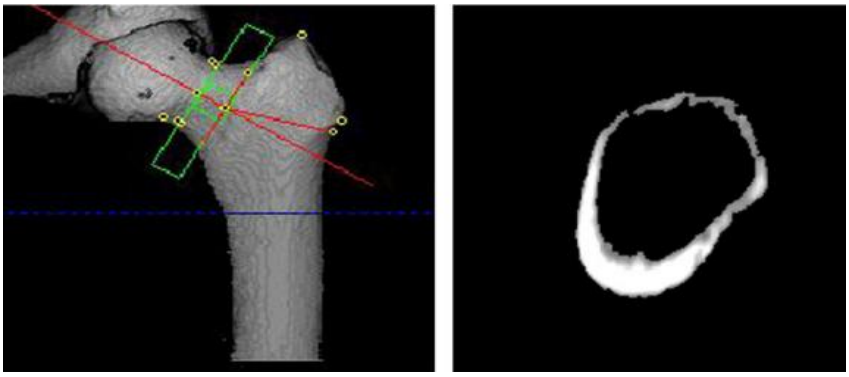

Figure 2-8 Left: CT scans of the proximal femur with defined longitudinal femoral neck axis, and showing the region of interest for cross section of the femoral neck; right: segmented cortical bone. (Adapted from Ito et al. [90])

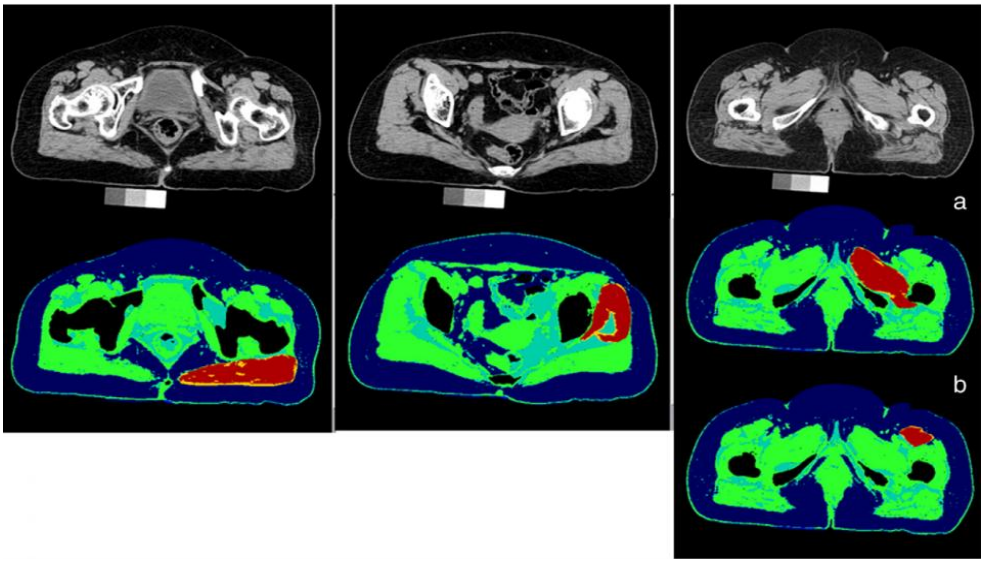

Figure 2-9 CT scans of hip muscles. Left: hip extensor; middle: abductor; right: (a) hip abductors and (b) hip flexors; Top grey images are raw CT scans; bottom colored images are software automatically segmented images combined with user manually correction: lean areas are shown in green, while fat areas outside and inside lean areas are shown in dark and light blue, respectively. Red areas are lean tissues that outlined for illustration and orange areas are fat tissues within the lean tissues. Black areas are bones. (by Lang et al. [96])

2.6.3 Magnetic Resonance Imaging (MRI)

Magnetic resonance imaging (MRI) is a 3D imaging technique that provides measurements of bone geometry and strength and soft tissues such as muscles; although it has some contraindications and limitations, it offers non-ionizing radiation to a subject which increases researchers' interest in investigating the potential of MRI in musculoskeletal measurements. MRI uses a powerful magnetic field to align the magnetization of some atomic nuclei in the body. Radio frequency pulses are applied to systematically alter the alignment of the magnetization. This causes the nuclei to produce a rotating magnetic field detectable by the scanner. At the final stage, MRI constructs an image of scanned area based on recorded information [103-104]. Unlike CT, MRI is capable of directly acquiring images of a 3D structure at arbitrary orientations without reformatting axial data [105]. With its 3D imaging ability, MRI has been used to measure bone geometry, estimate bone strength and investigate bone changes at the proximal femur [9, 106]. MRI has been generally applied to depict cortical and trabecular bone, thus, bringing the scope down to the macrostructure of femur [105-108]. In addition, MRI is uniquely suited for muscle area measurement due to its superior soft tissue contrast that makes the measurement of soft tissue feasible. Although MRI has some contraindications (patients with a pacemaker are not allowed to take MRI scans) and limitations (high cost and long imaging time), researchers continue to investigate MRI performance (i.e. repeatability) because of non-ionizing radiation and superior soft tissue contrast features [9, 62, 75, 78, 106, 108].

To date, the performance of MRI has been investigated in regard to bone geometry, strength and muscles area at the lower limb (Figure 2-10 and 2-11) [9, 75, 105-106, 109]. Sievanen et al. [9] conducted the most comprehensive MRI precision study so far, but through this study he only focused on measurement of the femoral neck (Figure 2-10). In this study, MRI images were

segmented manually, which resulted in high values of precision errors (i.e. root mean square coefficient of variation; CV_{rms}%) for bone strength measures. Also, he obtained CV_{rms}% for polar section modulus and cortical-to-total ratio as the only two measures of the bone strength. However, in the majority cases, the proximal femur is subjected to bending and compression. Polar section modulus is the bone strength index in torsion and cortical-to-total ratio is essentially the area-based buckling ratio which is the bone strength index in compression. The bone strength index in bending was not reported in this study. In addition, image analysis applied in this study was based on assuming the cross section of the femoral neck is a circular shape, which also increased CV_{rms}% because the femoral neck is a non-symmetrical structure [9]. Woodhead et al. [109] conducted a MRI precision study focused on the bone geometry of the midfemoral shaft. However, this study reported coefficient of variation (CV%) as precision results. CV% is only the representative of the short-term precision of an individual subject, which cannot represent the performance of the technique in general. Instead, CV_{rms}% was suggested for calculating the short-term precision of an imaging technique [110]. Also in this study, the performance of MRI on measuring the femoral shaft strength properties was not included [109]. This is insufficient to estimate the bone condition as the bone strength is the direct measure rather than the bone geometry. To our knowledge, there is no MRI precision study that evaluates the surrounding muscle area of the proximal femur. There was only one study which reported the performance of MRI on measuring the muscle volume at the leg [75] (Figure 2-11). This study only used the intraclass correlation coefficients (ICC) to define the repeatability of MRI. This is insufficient to characterize the repeatability of an imaging technique as ICC only refers to how strongly variables resemble each other.

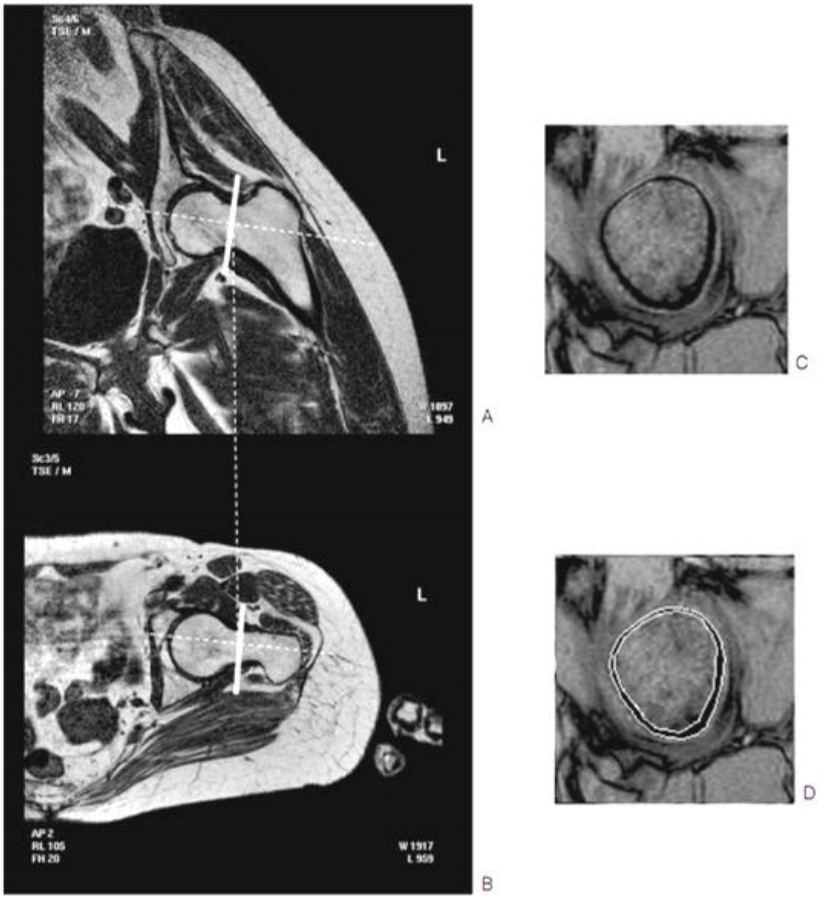

Figure 2-10 MRI images of the proximal femur in (A) oblique coronal and (B) oblique saggital directions; (C) raw MRI image of the femoral neck; (D) with manual delineation of periosteal and endosteal boundaries [9].

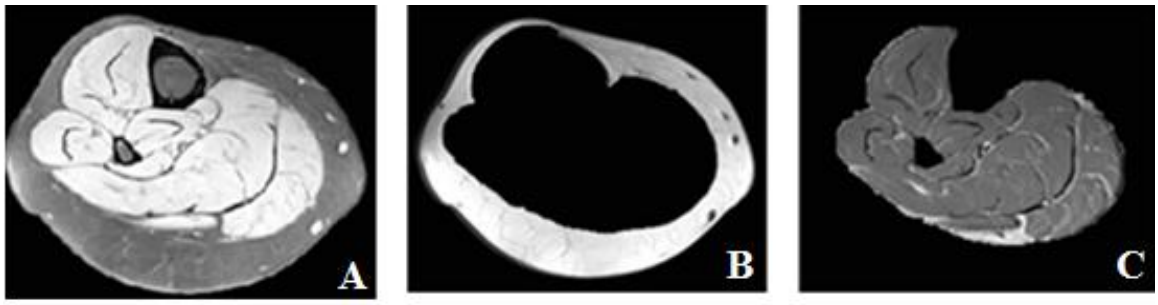

Figure 2-11 (A) MRI image of calf muscles at leg; (B) segmented subcutaneous fat; (C) segmented calf muscles. (Adapted from Commean et al. [75])

2.7 Summary

1. Hip fractures are most common to the population characterized by weakened bone and muscle strength, such as elderly people; the strength of femoral neck and shaft is associated with increasing risk of hip fractures.

2. Bone geometry is an important determinant of bone strength.

3. Muscles affect bone through bone-muscle interactions, and contribute towards preventing fall-related hip fractures. Muscle area is a surrogate measure of muscle force.

4. The most popular imaging techniques for bone and muscle are DXA and CT. These methods have certain limitations: DXA is limited to estimations of bone and muscle structure from 2D scans; and CT delivers high radiation dose which could be harmful for participant's health.

5. MRI is able to measure bone and muscle in 3D without radiation exposure. However, its performance at measuring the proximal femur and surrounding muscle properties is under-explored.

3 RESEARCH QUESTIONS AND OBJECTIVES

3.1 Research Questions

The basic question which motivates my M.Sc. research is: Can MRI precisely measure proximal femoral bone and muscle properties. To help answer this basic question, the goal of my M.Sc. research was to determine the precision (i.e. repeatability) of MRI-based measures of bone and muscle properties. Using MRI, in combination with custom imaging processing algorithms, I aimed to answer the following research questions:

1. Can MRI provide precise *in vivo* measures of bone geometry and strength of the femoral neck and shaft?

2. Can MRI provide precise *in vivo* measures of muscle area at the femoral shaft?

3.2 Research Objectives

To answer the questions posed in this study, my objectives were to:

1. Determine the *in vivo* precision of MRI in deriving bone geometry and estimating bone strength at the femoral neck and shaft.

2. Determine the *in vivo* precision of MRI in measuring muscle area at the femoral shaft.

4 METHODS

4.1 Participants

Fourteen healthy participants (5M:9F) from the University of Saskatchewan were recruited for MRI scanning, with ages ranging from 21 to 68 years (mean±standard deviation (SD): 30.4±12.0 years). The participants provided consent for scanning. Due to unexpected reasons, the data of one participant were missing for the precision study of the femoral shaft and muscles. Without this participant, the age range of the new group of participants still remained the same, but the mean and SD shifted a little (mean±SD: 30.6±12.5 years).

4.2 MRI Acquisition

MRI scanning of the left hip and shaft was performed using a 1.5 MRI (MAGNETOM Avanto, Siemens, Muenchen, Germany) with body coil positioned over the hip and shaft regions. During scanning, the participants were positioned supine with legs extended and 15° externally rotated. For hip scan (i.e. femoral neck scan), a localizer scan using a T1-weighted spin-echo sequence (with parameters: TR=8.2ms, TE=3.51ms, number of excitation=1, flip angle=20°, slice thickness=6mm, in-plane pixel size=0.78x0.78 mm) was applied in oblique coronal and oblique saggital directions to determine the orientation of the femoral neck axis. Then a T1-weighted fast field-echo sequence was applied (with parameters: TR=12.7ms, TE=7.14ms, number of excitation=3, flip angle=10°, slice thickness=5mm, in-plane pixel size=0.49x0.49 mm) in a plane perpendicular to the oblique femoral neck axis (Figure 4-1). Thus the image plane represents the cross section of the femoral neck. For shaft scan, transverse images of the proximal femur

(relative to participant-specific orientation) were obtained using a T1-weighted turbo spin-echo sequence (with parameters: TR=616ms, TE=12ms, number of excitation=2, flip angle=180°, slice thickness=4mm, in-plane pixel size=0.45x0.45 mm). A single trained technician took three scans of each region for each participant with repositioning: participants were required to take a short walk between scans to incorporate the effects of different positioning and scanning orientation on precision outcomes. Each hip or shaft scan took 5min. The whole MRI scanning time was about 15min/measurement/participant, including participant preparation, two localizer scans and two study images (hip and shaft scans).

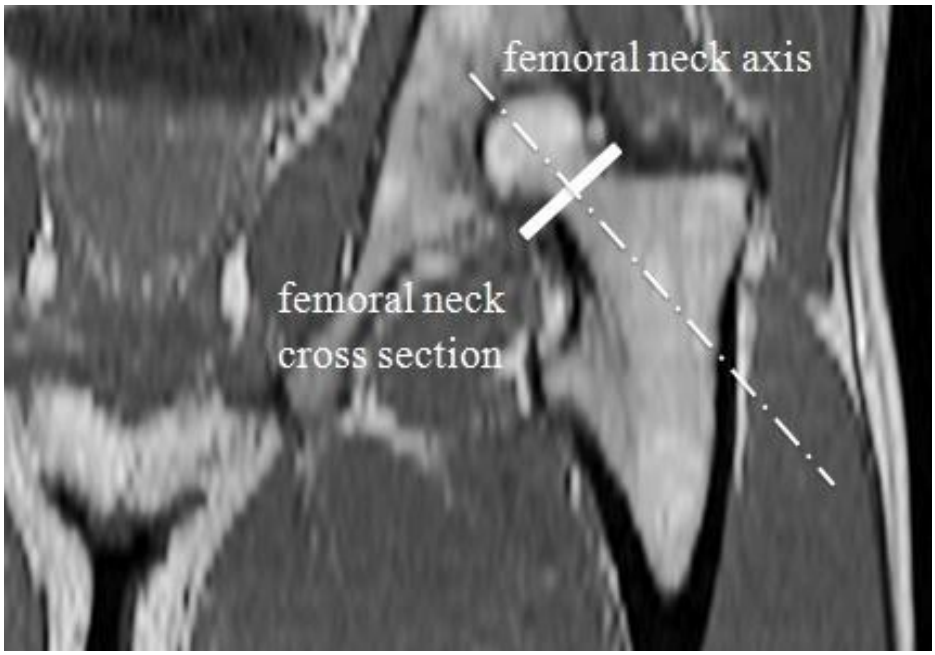

Figure 4-1. A localizer scan was first applied to find the femoral neck axis. Then scans of the cross section of the femoral neck were taken perpendicular to the neck axis.

4.3 Image Processing

4.3.1 Image Interpolation

Image interpolation was applied to original MRI images in order to transform a discrete image to a continuous image. The process of interpolation is to find the information for undefined or missed pixels based on the information provided by given pixels [111]. By applying image interpolation, the apparent stair-step effect of pixels can be reduced and smooth out the edges of pixels (Figure 4-2 and Figure 4-3). The interpolated image is closer to the actual image of the structure. In this study, image interpolation was applied to the shaft scans. The hip scans were not interpolated because the cortical thickness is so thin (e.g. ~1 mm or two pixels in parallel) that interpolated image may bring errors to precision results, such as including incorrect pixels (e.g. surrounding soft tissue pixels) as a part of bone.

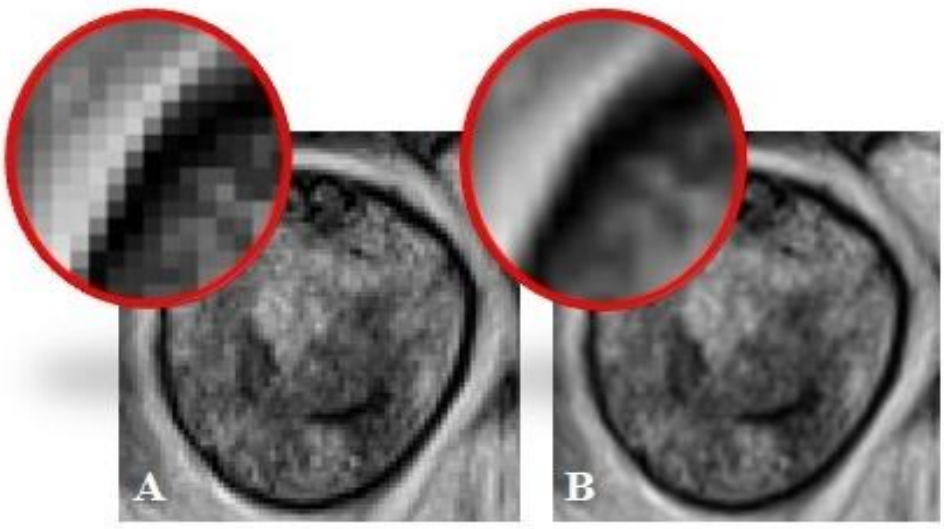

Figure 4-2. MRI images of the cross section of the femoral neck: (A) non-interpolated image (stair-step effect of pixels); (B) interpolated image (smooth boundary).

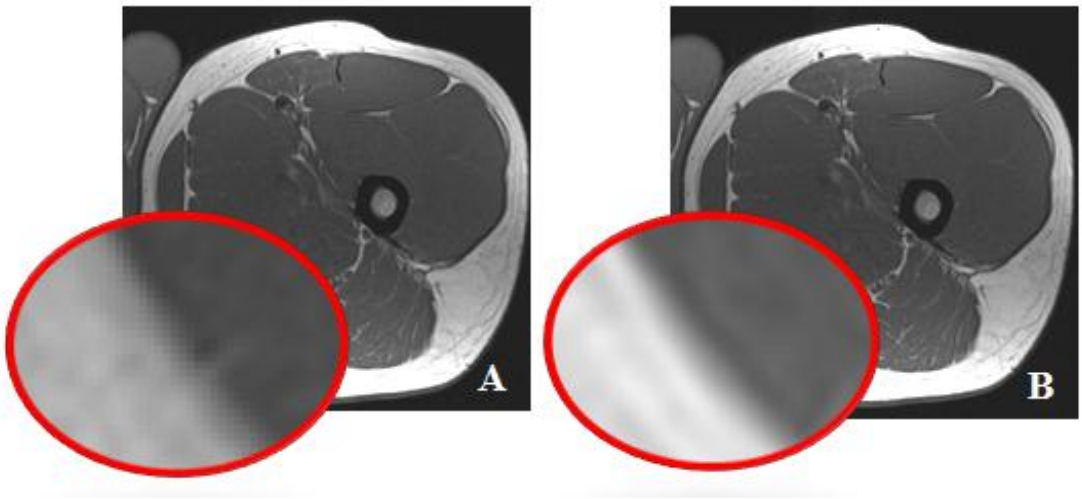

Figure 4-3. MRI images of the cross section of the femoral shaft and surrounding muscles: (A) non-interpolated image (stair-step effect of pixels); (B) interpolated image (smooth boundary).

4.3.2 Regions of Interest Selection

4.3.2.1 Femoral Neck Selection

In this study, the femoral neck was determined as the narrowest cross-section of the proximal femur from the hip scans [9]. By viewing the images along the femoral neck axis and comparing the cross sectional areas of the femoral neck region, the one with the narrowest cross section was chosen.

4.3.2.2 Femoral Shaft Selection

The location of the femoral shaft was determined as being 2cm below the transition site (observed in the transverse images) between the proximal femur and femoral shaft (Figure 4-4) [112]. The transition site is determined as being where the cross section of the proximal femur just being a circular-like shape. Because the shaft scans were interpolated, the overall volume was divided

into more image slices, e.g. the image analysis software automatically divided 37 image slices to 329 image slices. Then each slice thickness decreased from 4mm to 0.45mm; and a distance of 2cm is equivalent to 45 interpolated image slices. Therefore, the 2cm location below the transition site was determined by moving 45 slices down from this point.

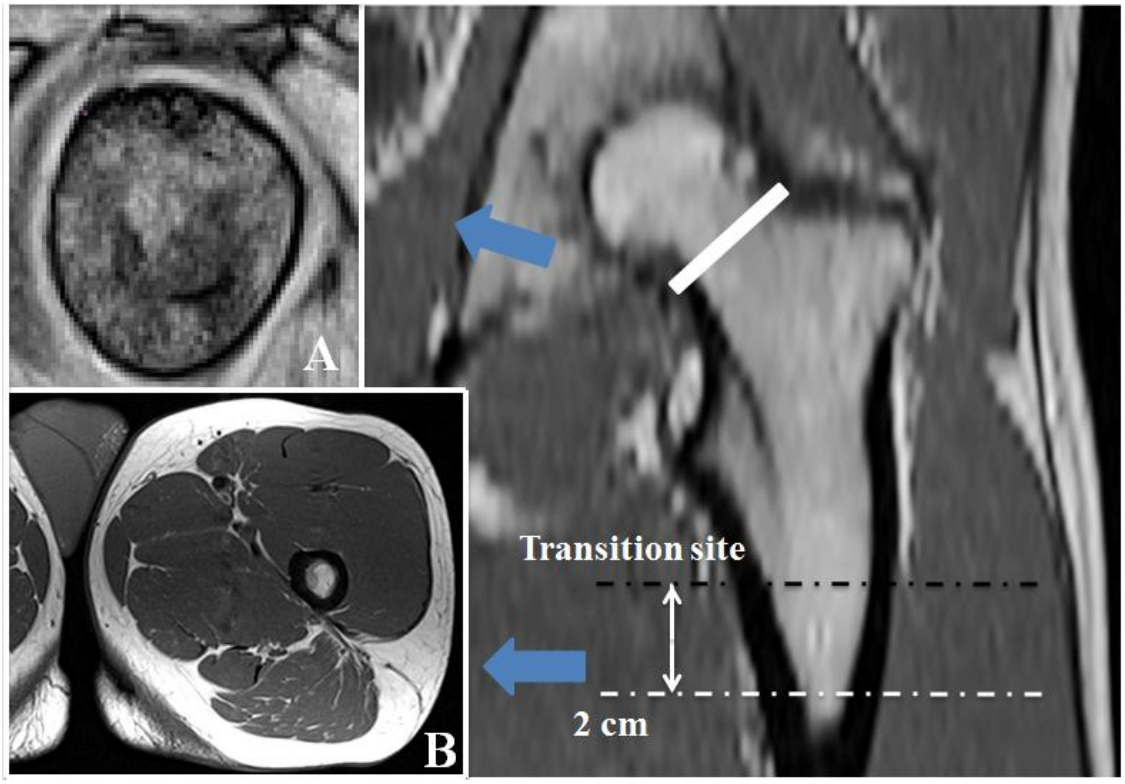

Figure 4-4. Illustration above shows the locations of femoral neck and shaft from this study. The location of femoral neck was chosen as the narrowest cross section (A) of the entire proximal femur. The location of femoral shaft was chosen as the cross section (B) at 2cm below the transition site between the proximal femur and femoral shaft.

4.3.2.3 Surrounding Muscle Groups

The location of the femur muscles was the same as that of the femoral shaft. In order to facilitate muscle delineation, four muscle groups were distinguished according to their movement functionalities (Figure 4-5): hip extensors (gluteus maximum, semitendinosus and biceps femoris long head), hip adductors (adductor magnus, adductor longus, adductor brevis and gracilis), hip flexors (rectus femoris and sartorius) and knee extensors (vastus intermedius, vastus medialis and vastus lateralis).

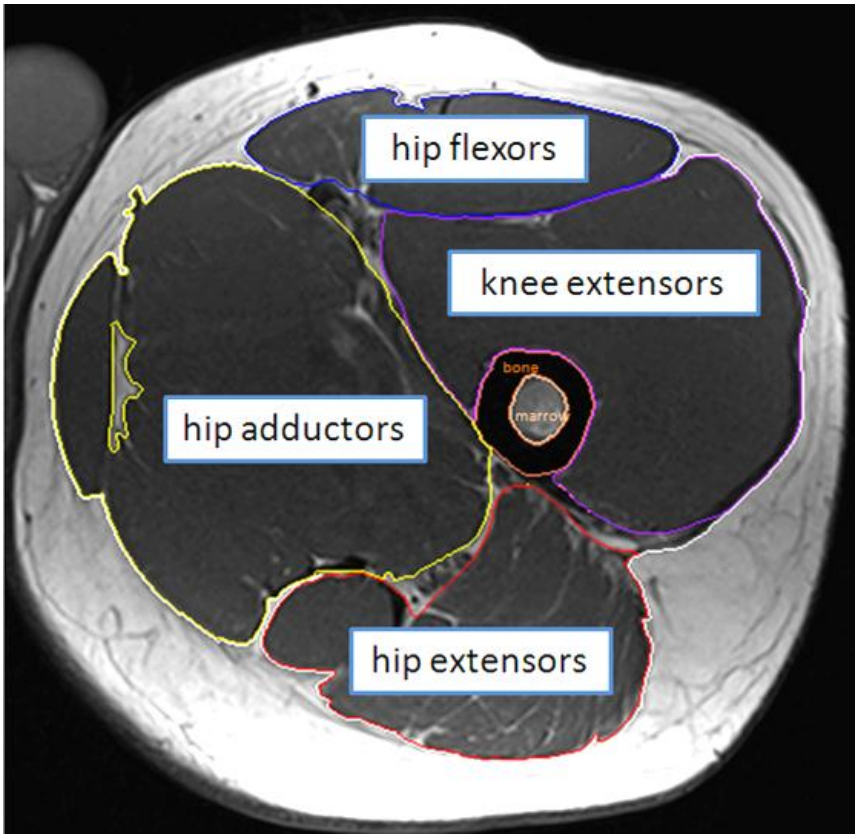

Figure 4-5. The surrounding muscles of the femoral shaft at 2cm below the transition site between the proximal femur and femoral shaft were divided to four groups: hip extensors (gluteus maximum, semitendinosus and biceps femoris long head), hip adductors (adductor magnus, adductor longus, adductor brevis and gracilis), hip flexors (rectus femoris and sartorius) and knee extensors (vastus intermedius, vastus medialis and vastus lateralis).

4.3.3 Image Segmentation

4.3.3.1 Half-Maximum-Height (HMH) Method

The Half-Maximum-Height (HMH) method is an approach to define a threshold for optimizing boundary delineation and minimizing manual corrections (i.e. reduce artificial errors) [113-114]. In this study, the subject-specific segmenting thresholds were defined using the HMH method. This approach defines the threshold as the midpoint between the maximum and minimum intensity on histogram line profiles of two adjacent regions of interest. For the femoral neck segmentation, the pixel intensities of trabecular bone, cortical bone and surrounding soft tissues were determined. The thresholds for delineating endosteal and periosteal boundaries were calculated by taking the average values of the pixel intensities of cortical bone/trabecular bone and cortical bone/surrounding soft tissue (i.e. capsular ligaments), respectively. For the femoral shaft segmentation, the pixel intensities of muscle, cortical bone and bone marrow were determined. The thresholds for delineating endosteal and periosteal boundaries were calculated by taking the average values of the pixel intensities of cortical bone/bone marrow and cortical bone/muscle, respectively. For the femur muscle segmentation, the pixel intensities of fat tissue and muscle were determined. The thresholds for delineating muscle group boundaries were calculated by taking the average values of the pixel intensities of fat tissue/muscle respectively.

4.3.3.2 Segmentation Procedures

MRI images were transferred to ANALYZE 10 (Mayo Foundation, Rochester, MB, USA), a commercially available software, for boundary delineation using semi-automatic region growing approach (Figure 4-6 and 4-7). Firstly, we placed a seed at the center of a region; secondly, we

grew the periosteal boundary of the cortical bone based on this seed, while adjusting pixel intensity until it reached the subject-specific threshold using HMH method; thirdly, we grew the endosteal boundaries of the cortical bone using the same approach; and finally, we manually corrected those two boundaries where necessary, in order to ensure the entire regions of interest were included. A touch-screen interactive tablet (Cintiq21uX, Wacom, Krefeld, Germany) was used to perform manual correction. Regarding to femoral neck and shaft delineations, the cortical areas were outlined with the assistance of endosteal and periosteal boundaries. Regarding to muscle delineation, intermuscular boundaries of the four muscle groups were outlined using the same approach.

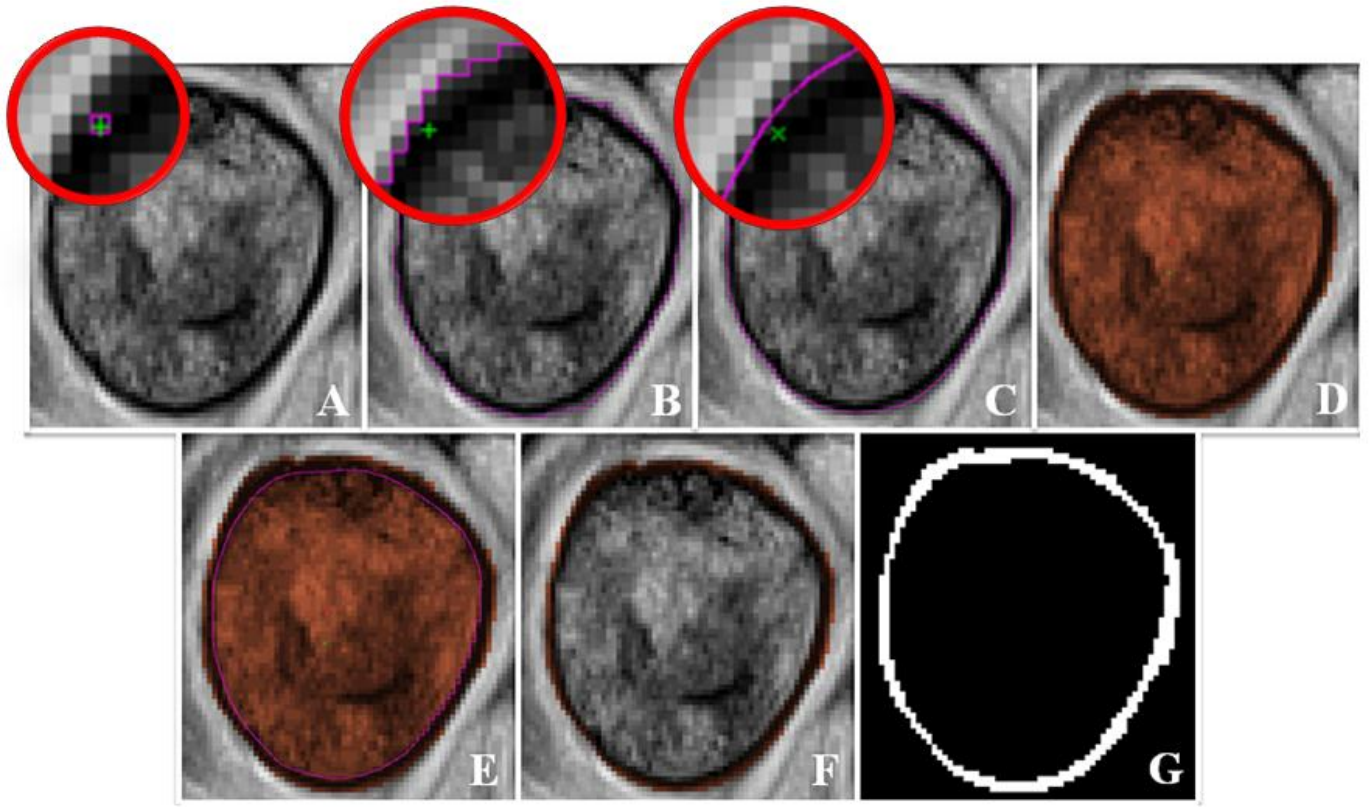

Figure 4-6 Illustration above shows semi-automatic segmentation process of MRI image of the femoral neck. In the process, we attempted to delineate the periosteal boundary by first placing a seed (A) at the middle of the black area (cortical area); we grew a boundary from this seed by applying threshold (B); we manually corrected the boundary where it was automatically over-outlined (C); we marked the whole region with coral color, which represents the total area of the femoral neck (D); using the same segmentation approach, we depicted the endosteal boundary (E); we outlined the cortical area with coral color by switching the trabecular area back to original color (F); the final presence of segmented MRI image, in which white colored area represents the cortical area (G).

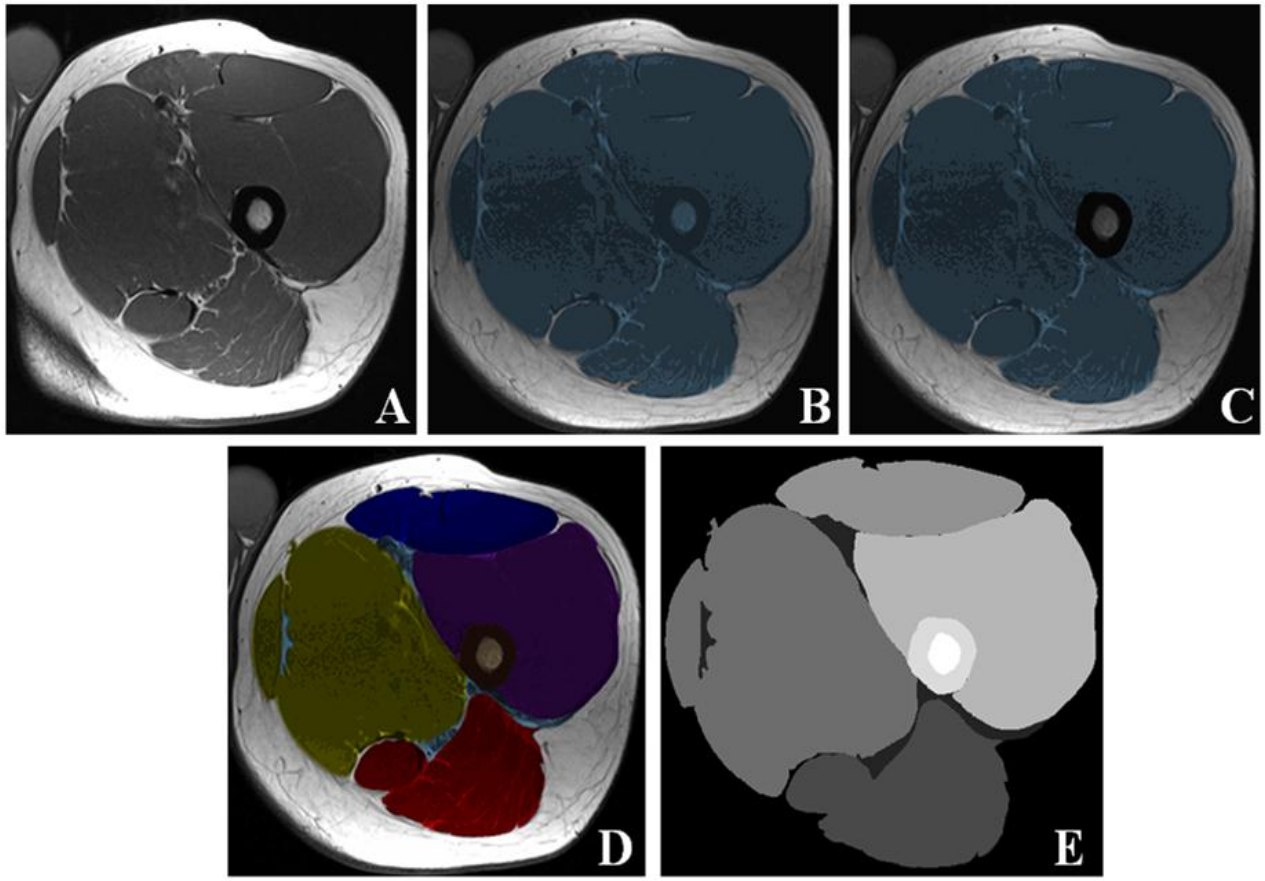

Figure 4-7 Illustration above shows the segmentation process of MRI image of the femoral shaft and surrounding muscles. Based on a raw MRI image (A), we outlined the whole area include total shaft and muscle area using the same segmentation process that applied to segment the femoral neck image (B); then, we excluded area of the total shaft (C); we outlined each muscle group, cortical and marrow cavity area using different color to distinguish (D); the final presence of segmented MRI image with areas showing in different grayscale (E).

4.4 Bone Geometry and Strength and Muscle Area

Custom algorithms (MATLAB, The Mathworks, Inc., Massachusetts, USA) was employed for extracting geometrical and strength properties from segmented images. The geometrical properties of proximal femoral neck and shaft include total area (A_{tot}), cortical area (A_{cor}), trabecular area (A_{trab}; for the femoral neck only) and cortical thickness (t) were extracted. A_{tot} referred to the area surrounded by the periosteal boundary; A_{cor} corresponded to the cross-sectional areas surrounded by the endosteal and periosteal boundaries; A_{trab} referred to the area surrounded by the endosteal boundary; we calculated t in using two different approaches: circular ring approach (t_c) and unrolling approach (t_u). The circular ring approach was based on assuming the cross section of the femoral neck is a circular shape, t was obtained by calculating the difference between the outer periosteal radius and inner endosteal radius; the unrolling approach was based on firstly unrolling the cortical bone to obtain a trapezoid-like shape, and this shape can be changed to a rectangle-like shape with the length being the average length of the periosteal and endosteal boundaries and width being the cortical thickness. Thus t_u was calculated by dividing A_{cor} by the average length of periosteal and endosteal boundaries. Regarding to muscle analysis, the areas of total muscle, hip extensors, hip adductors, hip flexors and knee extensors were extracted. The strength properties include principal moment of inertia (I_{max} and I_{min}), sectional modulus (Z_{max} and Z_{min}), torsional rigidity (Z_p; for the femoral neck only) and buckling ratio (BR) were calculated according to those equations listed in section 2.4 of chapter 2.

4.5 Statistical Analysis

The *in vivo* precision of MRI-derived measures was defined by calculating the average root mean square coefficient of variation (CV_{rms}%) [110]. CV_{rms}% is the accurate assessment of the short-term precision error of an imaging technique, and low CV_{rms}% is an indication of high precision of this technique [110]. There is no critical CV_{rms}% value to quantify if the technique has high precision. However, the Least Significant Change (which equals to 2.77 times CV_{rms}%) is used to define if a difference (or change) between two measures is due to a true difference or due to imprecision of the technique [115]. For example, for a measure with a CV_{rms}% value of 5%, if the observed difference is greater than 2.77x5%=13.9%, one can conclude that the difference is true and not due to imprecision associated with the technique. In this study, we scanned 14 participants with three times each, achieving 28 degrees of freedom (DOF). The total number of 42 scans was to ensure this study meet a requirement of minimum of 27 DOF, which is considered to be sufficient for charactering technique's imprecision (i.e. a level of an upper 90% confidence limit of +30% of the mean precision error) [110]. The mean, standard deviation (SD) and ranges were also generated as descriptive data.

4.6 Results

In vivo precision errors (i.e. CV_{rms}%) for MRI-derived bone and muscle outcomes were small (i.e. <7.6%). At the femoral neck, CV_{rms}% for bone area ranged between 1.8% (A_{tot} and A_{trab}) to 5.3% (A_{cor}); CV_{rms}% for cortical thickness varied from 5.0% (t_u) to 5.9% (t_c); CV_{rms}% for bone strength ranged between 4.9% (BR) to 7.6% (Z_{max}) (Table 4-1). At the femoral shaft, CV_{rms}% for bone

area ranged between 1.2% (A_{tot}) to 1.7% (A_{cor}); CV_{rms}% for cortical thickness varied from 1.7% (t_u) to 2.0% (t_c); CV_{rms}% for bone strength ranged between 2.0% (Z_{min}) to 3.1% (I_{max}) (Table 4-2). For muscle area, CV_{rms}% ranged between 1.3% (total muscle area) to 4.5% (hip extensor area) (Table 4-3).

Table 4-1 Precision results for 1.5T MRI-derived bone geometrical and strength properties of the proximal neck. Geometrical properties include total bone area (A_{tot}), cortical area (A_{cor}), trabecular area (A_{trab}) and cortical thickness (t); strength properties include principal moment of inertia (I_{max} and I_{min}), section modulus (Z_{max} and Z_{min}), polar section modulus (Z_p) and buckling ratio (BR). Precision is reported using root mean square coefficient of variation (CV_{rms}%).

	NECK											
	Geometrical properties					Strength properties						
	A_{tot} (mm^2)	A_{cor} (mm^2)	A_{trab} (mm^2)	t_c (circular) (mm)	t_u (unrolling) (mm)	I_{max} (mm^4)	I_{min} (mm^4)	Z_{max} (mm^3)	Z_{min} (mm^3)	Z_p (mm^3)	BR (classic)	BR (area-based)
Mean	736.0	128.3	607.9	1.5	1.4	16667.3	11407.5	922.1	735.4	1880.2	13.4	5.8
SD_{rms}	12.4	6.4	10.2	0.1	0.1	1143.4	694.5	65.7	47.7	102.0	0.7	0.3
CV_{rms}%	1.8	5.3	1.8	5.9	5.0	7.3	6.5	7.6	6.9	5.8	5.4	4.9

Table 4-2 Precision results for 1.5T MRI-derived bone geometrical and strength properties of the proximal shaft. Geometrical properties include total bone area (A_{tot}), cortical area (A_{cor}) and cortical thickness (t); strength properties include principal moment of inertia (I_{max} and I_{min}), section modulus (Z_{max} and Z_{min}) and buckling ratio (BR). Precision is reported using root mean square coefficient of variation (CV_{rms}%).

	SHAFT									
	Geometrical properties				Strength properties					
	A_{tot} (mm^2)	A_{cor} (mm^2)	t_c (circular) (mm)	t_u (unrolling) (mm)	I_{max} (mm^4)	I_{min} (mm^4)	Z_{max} (mm^3)	Z_{min} (mm^3)	BR (classic)	BR (area-based)
Mean	632.4	434.1	6.4	6.3	34515.4	24248.7	2155.9	1768.0	2.6	1.5
SD_{rms}	7.8	7.5	0.1	0.1	1070.3	690.4	61.3	35.0	0.1	0.0
CV_{rms}%	1.2	1.7	2.0	1.7	3.1	2.8	2.8	2.0	2.7	1.4

Table 4-3 Precision results for 1.5T MRI-derived muscle areas at the femur (2cm below the transition site between the proximal femur and femoral shaft). Muscle areas include the areas of total muscles and four muscle groups (hip extensors, hip adductors, hip flexors and knee extensors). Precision is reported using root mean square coefficient of variation (CV_{rms}%).

	Total muscles (mm^2)	MUSCLE GROUPS			
		Hip extensors (mm^2)	Hip adductors (mm^2)	Hip flexors (mm^2)	Knee extensors (mm^2)
Mean	14348.3	2830.0	5462.2	1583.0	3838.4
SD_{rms}	180.0	127.5	86.8	28.5	69.5
CV_{rms}%	1.3	4.5	1.6	1.8	1.8

5 DISCUSSION

5.1 Overview of Findings

In this thesis research, we assessed the performance of MRI on measuring the proximal femur and surrounding muscles. This is the first MRI precision study that includes the measures of bone's principal moment of inertia (I_{max} and I_{min}), section modulus (Z_{max} and Z_{min}) and the area of muscle groups.

This research shows that MRI is precise in measuring bone geometry, strength and muscle area at the proximal femur, *in vivo*. The *in vivo* precision errors reported in this research represent the worst-case scenario, because they took participant repositioning and artificial movement errors into account. This research shows that the average CV_{rms}% for bone measures was less than 4.0%, and that for muscle measures was less than 2.5%. According to the Least Significant Change, on average, MRI is able to measure change in bone and muscle measures if the change is more than 11.1% and 7.0%, respectively [115]. Low precision error values are contributed by the HMH method and semi-automatic region-growing segmentation, which facilitated the boundary discrimination and eliminated the majority of error sources result from fully manual image segmentation. Particularly, the precision error values for muscle measures were lower, which is due to MRI unique ability to display superior soft tissue contrast [116]. This ability of MRI is useful to differentiate muscle from bone and subcutaneous adipose tissue, and also showing more muscle details than CT and DXA do, such as clear presence of intramuscular adipose tissues. Meanwhile, higher CV_{rms}% was found for estimating bone strength using MRI (average CV_{rms}%: 4.8%), which indicates that MRI is still able to measure change in bone strength as long as that change (or difference) is more than 13.3% [115]. Basically, the bone

strength is calculated from more than one geometrical property; however, each geometrical property has already been associated with certain amount of precision errors. Statistically, those precision errors accumulate if more than one variable (e.g. geometrical properties) involves, which increases the bone strength precision errors. Our results identify the potential of MRI in estimating bone strength and muscle area at the proximal femur.

5.2 Comparison to Existing Findings

In comparison with existing studies, our precision results for geometry-based bone outcomes compare favorably with *in vivo* measurements using MRI [9, 62, 75, 106, 109]. At the femoral neck, total cross-sectional area CV_{rms}% was 1.8%, which compares with previous findings ranging from 1.4% to 2.7% [9, 62, 106]; and cortical area CV_{rms}% was 5.3%, which compares with findings ranging from 5.4% to 11.7% [9, 62, 106]. Precision results for geometry and strength calculations which involved mathematical calculations, however, differed from previous results. Mean cortical thickness CV_{rms}% results (circular: 5.9%, unrolling: 5.0%) were smaller than previous results ranging from 11-13.2% using the circular approach [9]. Buckling ratio CV_{rms}% results (area-based: 4.9%, classic: 5.4%) were smaller than previous results from 7.3% to 9.9% using an inverse of the area-based approach [9]; and Z_p CV_{rms}% was 5.8%, which was smaller than previous findings ranging from 12.5-15.1% [9]. Our smaller precision errors are likely attributed to the usage of subject-specific thresholds and semi-automatic region-growing segmentation with minimal user correction (e.g. via interaction pen) whereas previous studies depended predominately upon manual segmentation [9, 62, 106]. In addition, unlike Sievanen et al. [9], the assumption of circular shape for calculating the cortical bone was avoided in this study.

In reality, the shape of femur varies and distributed asymmetrically [22]. With regards to the muscle area, to our knowledge no MRI-based studies have determined precision errors for muscle areas of the thigh. However, our muscle area CV_{rms}% results (range: 1.3%-4.5%) compare with CT-based precision errors ranging from 3.3% to 9.4% for hip extensor and flexor area [76]. Our CV_{rms}% results compensate the lack of evaluation for the short-term MRI performance on estimating bone strength of the femoral shaft and area of surrounding muscles.

In comparison with previous studies using other imaging techniques, such as DXA and CT, our MRI precision errors were lower than DXA-based HSA precision errors and comparable with CT precision errors. At the femoral neck, MRI-based bone geometry CV_{rms}% results (range: 1.8%-5.9%) compare with HSA-based results (range: 2.1%-7.9%) [117] and CT-based results (total area: 0.8%; cortical thickness: 1.5%) [93, 95]; MRI-based bone strength CV_{rms}% results (range: 5.4%-7.6%) compare with HSA-based results (range: 3.4%-11.7%) [117]. At the femoral shaft, MRI-based bone geometry CV_{rms}% results (range: 1.2%-2.0%) compare with HSA-based results (range: 0.9%-4.2%) [117] and CT-based results were lacked; MRI-based bone strength CV_{rms}% results (range: 2.0%-3.1%) compare with HSA-based results (range: 2.5%-5.1%) [117]. Although, the changes of the CT-based bone strength at the femoral neck and shaft were investigated [48], corresponding precision results were lacked.

5.3 Strengths and Limitations

5.3.1 Study Strength

This thesis research has various strengths related to clinical application of MRI technique and study design, which require further explanation or have not yet been discussed.

MRI possesses unique advantages for its clinical application, which makes its usage as one of study strengths. First, MRI is able to measure body extremity in arbitrary orientation. This ability allows it to measure proximal aspect of the femur – hip region, especially the femoral neck which is located deeply at the hip region with femoral neck axis has certain angle to shaft axis [118]. This is important because the femoral neck is a vital region in determining the theoretical fracture threshold for the entire femur [9]. Second, MRI offers superior soft tissue contrasts that can clearly manifest regions of bone and muscle [116]. The distinguishable boundaries of bone-muscle facilitate region recognition and segmentation process. This ability allows more confident and precise measurement of bone-muscle structure. Third, MRI exposes no ionizing radiation to measuring subject and environment. This huge advantage keeps MRI away from ethical issue for *in vivo* measurements. So far, none of other imaging techniques possesses this advantage.

The key strength of this research is the inclusion of femoral neck, shaft and surrounding muscles as the regions of interest, which makes this research to be comprehensive to assess the *in vivo* performance of MRI at the proximal femur for popular fracture instances. Those regions are commonly related to the risk of hip fracture, such as femoral neck fracture and shaft fracture usually happen with different impact instances [17-18, 49]. It is also important to include the measurement of surrounding muscles, because it is believed that hip fracture is not only related to bone strength but also muscle area [4-5, 35-36]. A second strength of this research is the

application of HMH method. Using this thresholding method, the majority amount of manual boundary delineation process was omitted. This method improved the precision by reducing the artificial errors that can deteriorate real estimation of MRI performance. A third strength of this research is that it is designed with adequate number of participants to define the short-term precision of an imaging technique. In this research, 14 participants were recruited and scanned three times using the same MRI equipment. Therefore, a total of 28 DOF were achieved to meet the requirement for estimating precision errors with an upper 90% confidence limit of less than 30%, which is a level considered sufficient for characterizing technique's imprecision [110].

5.3.2 Study Limitations

This research has study limitations pertaining to participants and unexpected data missing. First, the participants recruited for this research were in healthy condition (i.e. they do not have problematic proximal femur and muscles), and our study sample was young with only one older participant (i.e. aged 68 years). However, older participants, especially the ones with osteoporotic bone or atrophic muscle, are usually associated with thin cortical bone and small muscle area, respectively, which may complicate image segmentation process and increase the precision error [9]. Our results therefore represent an ideal case. Second, the shaft and muscle data of one participant were missing, which lowered the DOF from 28 to 26. Although the desired DOF is 27 for adequately assessing the short-term precision of an imaging technique, 26 DOF does not make a huge difference in the results. For example, instead of estimating the precision errors with an upper 90% confidence limit of approximately +29%; with 26 DOF, we are still able to estimate the precision errors with an upper 90% confidence limit of approximately +31% [110].

5.3.3 Technical Limitations

This research has technical limitations related to boundary delineation and time consumption. The primary technical limitation is relevant to segmentation obstacles that arise from 1) the trabecular bone or bone marrow adjacent to the endosteum at the femoral neck and shaft; 2) the hip extensors muscle group that contains massive intramuscular adipose tissues. First, the healthy, young to middle-aged participants commonly contain substantial amounts of hematopoietic red bone cells within the trabecular area and the bone marrow cavity. This natural phenomenon may complicate the discrimination of endosteal boundary from trabecular area (i.e. for the femoral neck segmentation) or bone marrow cavity (i.e. for the femoral shaft segmentation), which majorly caused failure to automatically delineate endosteal boundary based on thresholding method only. In this case, manual segmentations were applied to correct the boundary where it is necessary, which also brought in errors. Second, similar obstacle was found when segmenting the hip extensors muscle group, as a large amount of intramuscular adipose tissues was observed. The boundary of the hip extensors was much harder to distinguish from surrounding adipose tissue than other muscle groups, which involved a larger amount of manual corrections and artificial errors. Third, the whole process of participant scanning was time consuming. MRI took about 5min for a length of 15cm hip scan. The scanning time is longer than CT uses, e.g. current CT takes only 80-200ms for one slice of scan, therefore, 24-60s for a 15cm hip scan [89]. The longer scanning time of MRI may increase concern for motion artifacts.

6 CONCLUSIONS AND FUTURE DIRECTIONS

6.1 Conclusions

In conclusion, the *in vivo* MRI precision study is among the most comprehensive in characterizing the proximal femur and its surrounding muscles. The precision results are comparable to those previously published MRI precision study, and complement the limited evidence of MRI-derived bone strength and muscle area measurements at the femoral shaft. Our results demonstrate that MRI is a promising non-ionizing technique for monitoring changes in bone geometry, strength and muscle area at the clinically important femoral neck and shaft.

6.2 Contributions

This study has generated several "firsts" (listed below), extending knowledge of MRI's potential on application of the proximal femur and surrounding muscles.

1. First study to include MRI-derived estimation of principal moment of inertia (I_{max} and I_{min}) and section modulus (Z_{max}) and (Z_{min}) as bone strength indices.

2. First study to evaluate MRI performance for estimating bone strength and muscle area at the femoral shaft.

6.3 Clinical Significance

The majority of hip fractures happen suddenly due to the compromised bone strength of the individuals cannot withstand a high impact. However, fragile bones develop silently and many people do not notice until hip fractures occur. An early diagnostic method is required. Current imaging techniques are limited in bone and muscle detections. Our results suggest that MRI has the potential to monitor small changes in bone geometry and strength and muscle area at the proximal femur, acting as a trustable imaging tool for early detection of fragile bone. Also, it is possible to investigate the influence of the bone geometry and the muscle area on the bone strength through measuring the changes, which will improve treatment of fragile bone.

6.4 Future Research

This thesis research has some potentials to improve regarding to selection of study participants, segmentation method, analysis processes and inclusion of adiposity measurement.

1. The participants recruited for this research were healthy, and most of whom were young to middle-aged. More complicated cases are suggested to be included for broadly accessing the performance of MRI, such as osteoporotic patients and/or elderly population who may have thinner cortical bone or more complex bone and muscle structures.

2. This research investigated the general performance of MRI, which incorporated the factors of mixed ethnics and genders. In the future study, MRI performance in regard to different ethnics and gender is recommended to assess separately.

3. The segmentation process could also be optimized by applying custom algorithm programming code for fully automatic segmentation, in order to eliminate errors brought by manual correction.

4. Regional analysis of bone's cross section is also recommended for future work. The bone geometry and strength of each region may differ to another because of asymmetrical distribution affected by lifelong daily physical activity.

5. It is noted that a decrease in skeletal muscle and an increase in adipose tissue accompanies increasing age [119-120]. This phenomenon may induce physical impairment and disability in elderly [121-122], and also associating with hip fracture [96]. Adiposity, or the percentage of fat tissues, is worth to estimate in the future in order to determine the effect of fat or lean tissue on the bone strength.

6. Validation of MRI technique is recommended for the future work. For bone measures, a comparison study can be conducted to find correlations between MRI-based measures and DXA or CT-based measures or mechanical testing-based cadaveric measures. For muscle measures, a comparison study can be conducted to find correlations between MRI-based measures and CT-based measures or dynamometry-based measures.

LIST OF REFERENCES

1. Cheng SY, Levy AR, Lefaivre KA, Guy P, Kuramoto L, Sobolev B, *Geographic trends in incidence of hip fractures: a comprehensive literature review.* Osteoporos Int., 2011. **22**(10): p. 2575-2586.
2. Wongtriratanachai P, Luevitoonvechkij S, Songpatanasilp T, Sribunditkul S, Leerapun T, Phadungkiat S, Rojanasthien S, *Increasing Incidence of Hip Fracture in Chiang Mai, Thailand.* J Clin Densitom, 2012: p. 1-6.
3. Kanis JA, Black D, Cooper C, Dargent P, Dawson-Hughes B, De Laet C, Delmas P, Eisman J, Johnell O, Jonsson B, Melton L, Oden A, Papapoulos S, Pols H, Rizzoli R, Silman A, Tenenhouse A, *A new approach to the development of assessment guidelines for osteoporosis.* Osteoporos Int., 2002. **13**(7): p. 527-536.
4. Ferretti JL, Cointry GR, Capozza RF, Frost HM, *Bone mass, bone strength, muscle-bone interactions, osteopenias and osteoporoses.* Mech Ageing Dev, 2003. **124**(3): p. 269-279.
5. Macdonald H, Kontulainen S, Petit M, Janssen P, McKay H, *Bone strength and its determinants in pre- and early pubertal boys and girls.* Bone, 2006. **39**(3): p. 598-608.
6. Järvinen TL, Sievänen H, Khan KM, Heinonen A, Kannus P, *Shifting the focus in fracture prevention from osteoporosis to falls.* BMJ, 2008. **336**(7636): p. 124-126.
7. Kannus P, Sievänen H, Palvanen M, Järvinen T, Parkkari J, *Prevention of falls and consequent injuries in elderly people.* Lancet., 2005. **366**(9500): p. 1885-1893.
8. Oliver D, Connelly JB, Victor CR, Shaw FE, Whitehead A, Genc Y, Vanoli A, Martin FC, Gosney MA, *Strategies to prevent falls and fractures in hospitals and care homes and effect of cognitive impairment: systematic review and meta-analyses.* BMJ, 2007. **334**(7584).
9. Sievanen H, Karstila T, Apuli P, Kannus P, *Magnetic resonance imaging of the femoral neck cortex.* Acta Radiol, 2007. **48**(3): p. 308-314.
10. Augat P, Eckstein F,, *Quantitative Imaging of Musculoskeletal Tissue.* Annual Review of Biomedical Engineering, 2008. **10**: p. 369-390.
11. Maughan RJ, Watson JS, Weir J, *Strength and cross-sectional area of human skeletal muscle.* J Physiol, 1983. **338**: p. 37-49.
12. Byrne DP, Mulhall KJ, Baker JF, *Anatomy & Biomechanics of the Hip.* The Open Sports Medicine Journal, 2010. **4**: p. 51-57.
13. Daniel M, I., Kralj-Iglič V, *The shape of acetabular cartilage optimizes hip contact stress distribution.* J Anat., 2005. **207**(1): p. 85-91.
14. Johnston JD, Noble PC, Hurwitz DE, Andriacchi TP, *Biomechanicas of the Hip. In: The Adult hip (Chap 5)*. 2nd ed, ed. R.A. Callaghan JJ, Rubash HE. 2007: Philadelphia, Lippincott Williams & Wilkins.
15. Gray H, *Gray's Anatomy*. 2008.
16. Zebaze RM, Jones A, Welsh F, Knackstedt M, Seeman E, *Femoral neck shape and the spatial distribution of its mineral mass varies with its size: clinical and biomechanical implications.* Bone, 2005. **37**(2): p. 243-252.
17. Rudman KE, Aspden RM, Meakin JR, *Compression or tension? The stress distribution in the proximal femur.* BioMedical Engineering Online, 2006. **5**(12): p. 1-7.
18. Taylor ME, Tanner KE, Freeman MAR, Yettram AL, *Stress and strain distribution within the intact femur: compression or bending?* Med. Eng. Phys., 1996. **18**(2): p. 122-131.
19. Andersson GB, Bouchard J, Bozic K, Campbell RM, Cisternas MG, Correa A, Cosman F, Cragan JD, D'Andrea K, Doernberg N, Dormans JP, Elderkin AL, Fershteyn Z, Gitelis S, Gnatz SM, Haralson RH, Helmick CG, Hochberg MC, Hu S, Katz JN, King T, Kirk R, *The Burden of Musculoskeletal Diseases in the United States*. second Edition ed. 2011.

20. Bell KL, Loveridge N, Power J, Garrahan N, Stanton M, Lunt M, Meggitt BF, Reeve J, *Structure of the femoral neck in hip fracture: cortical bone loss in the inferoanterior to superoposterior axis.* J Bone Miner Res, 1999. **14**(1): p. 111-119.
21. Crabtree N, Loveridge N, Parker M, Rushton N, Power J, Bell KL, Beck TJ, Reeve J., *Intracapsular hip fracture and the region-specific loss of cortical bone: analysis by peripheral quantitative computed tomography.* J Bone Miner Res, 2001. **16**(7): p. 1318-1328.
22. Mayhew PM, Thomas CD, Clement JG, Loveridge N, Beck TJ, Bonfield W, Burgoyne CJ, Reeve J., *Relation between age, femoral neck cortical stability, and hip fracture risk.* Lancet, 2005. **366**(9480): p. 129-135.
23. Cousins JM, Petit MA, Paudel ML, Taylor BC, Hughes JM, Cauley JA, Zmuda JM, Cawthon PM, Ensrud KE, *Muscle power and physical activity are associated with bone strength in older men: The osteoporotic fractures in men study.* Bone, 2010. **47**(2): p. 205-211.
24. McGlasson R, Zellermeyer V, MacDonald V, Lo N, Spafford D, McMullan JL, Beaupre L, Gould JS, Saryeddine T, Scott V, *National hip fracture toolkit*, B.a.J.D. Canada, Editor. 2011.
25. Osteoporosis Canada, *Osteoporosis Facts & Statistics*. 2011.
26. Cummings SR, Nevitt MC, Browner WS, Stone K, Fox KM, Ensrud KE, Cauley J, Black D, Vogt TM, *Risk factors for hip fracture in white women. Study of Osteoporotic Fractures Research Group.* N Engl J Med, 1995. **332**(12): p. 767-773.
27. Johnell O, Gullberg B, Kanis JA, Allander E, Elffors L, Dequeker J, Dilsen G, Gennari C, Lopes Vaz A, Lyritis G, et al., *Risk factors for hip fracture in European women: the MEDOS Study. Mediterranean Osteoporosis Study.* J Bone Miner Res, 1995. **10**(11): p. 1802-1815.
28. Miller PD, Siris ES, Barrett-Connor E, Faulkner KG, Wehren LE, Abbott TA, Chen YT, Berger ML, Santora AC, Sherwood LM, *Prediction of fracture risk in postmenopausal white women with peripheral bone densitometry: evidence from the National Osteoporosis Risk Assessment.* J Bone Miner Res, 2002. **17**(12): p. 2222-2230.
29. Albrand G, Munoz F, Sornay-Rendu E, DuBoeuf F, Delmas PD, *Independent predictors of all osteoporosis-related fractures in healthy postmenopausal women: the OFELY study.* Bone, 2003. **32**(1): p. 78-85.
30. Wehren LE, Magaziner J, *Hip fracture: Risk factors and outcomes.* Curr Osteoporos Rep, 2003. **1**(2): p. 78-85.
31. Lee SH, Lee TJ, Cho KJ, Shin SH, Moon KH, *Subsequent Hip Fracture in Osteoporotic Hip Fracture Patients.* Yonsei Med J, 2012. **53**(5): p. 1005-1009.
32. Li GW, Chang SX, Xu Z, Chen Y, Bao H, Shi X, *Prediction of hip osteoporotic fractures from composite indices of femoral neck strength.* Skeletal Radiol, 2013. **42**(2): p. 195-201.
33. Löfman O, Hallberg I, Berglund K, Wahlström O, Kartous L, Rosenqvist AM, Larsson L, Toss G., *Women with low-energy fracture should be investigated for osteoporosis.* Acta Orthop, 2007. **78**(6): p. 813-821.
34. Leavy B, Aberg AC, Melhus H, Mallmin H, Michaëlsson K, Byberg L, *When and where do hip fractures occur? A population-based study.* Osteoporos Int., 2013.
35. Trudelle-Jackson E, Jackson AW, Morrow JR, *Muscle Strength and Postural Stability in Healthy, Older Women: Implications for Fall Prevention.* Journal of Ohysical Activity and Health, 2006. **3**: p. 292-303.
36. Lastayo PC, Ewy GA, Pierotti DD, Johns RK, Lindstedt S, *The Positive Effects of Negative Work: Increased Muscle Strength and Decreased Fall Risk in a Frail Elderly Population.* Journal of Gerontology: Medical Sciences, 2003. **58A**(5): p. 419-424.
37. Kontulainen SA, Hughes JM, Macdonald HM, Johnston JD, *The biomechanical basis of bone strength development during growth.* Med Sport Sci., 2007. **51**: p. 13-32.
38. Beck, T., *Extending DXA beyond Bone Mineral Density: Understanding Hip Structural Analysis.* Curr Osteoporos Rep, 2007. **5**(2): p. 49-55.

39. Lau AN, Adachi JD, *Geriatric Rheumatology: A Comprehensive Approach - Chapter 2 Bone Aging*, ed. Nakasato Y, Yung RL. 2011: Springer Science + Business Media.
40. Szulc P, Seeman E, Duboeuf F, Sornay-Rendu E, Delmas PD, *Bone fragility: failure of periosteal apposition to compensate for increased endocortical resorption in postmenopausal women.* J Bone Miner Res, 2006. **21**(12): p. 1856-1863.
41. Dickenson RP, Hutton WC, Stott JR, *The mechanical properties of bone in osteoporosis.* J Bone Joint Surg Br, 1981. **63-B**(2): p. 233-238.
42. Chen H, Zhou X, Fujita H, Onozuka M, Kubo KY, *Age-related changes in trabecular and cortical bone microstructure.* Int J Endocrinol, 2013.
43. D'Elia G, Caracchini G, Cavalli L, Innocenti P, *Bone fragility and imaging techniques.* Clin Cases Miner Bone Metab., 2009. **6**(3): p. 234-246.
44. Kanis JA, *Diagnosis of osteoporosis and assessment of fracture risk.* Osteoporosis 2002. **359**: p. 1929-1936.
45. Stone KL, Seeley DG, Lui LY, Cauley JA, Ensrud K, Browner WS, Nevitt MC, Cummings SR, *BMD at multiple sites and risk of fracture of multiple types: long-term results from the Study of Osteoporotic Fractures.* J Bone Miner Res, 2003. **18**(11): p. 1947-1954.
46. Schuit SC, Van der Klift M, Weel AE, De Laet CE, Burger H, Seeman E, Hofman A, Uitterlinden AG, Van Leeuwen JP, Pols HA, *Fracture incidence and association with bone mineral density in elderly men and women: the Rotterdam Study.* Bone, 2004. **34**(1): p. 195-202.
47. Siris ES, Chen YT, Abbott TA, Barrett-Connor E, Miller PD, Wehren LE, Berger ML, *Bone mineral density thresholds for pharmacological intervention to prevent fractures.* Arch Intern Med., 2004. **164**(10): p. 1108-1112.
48. Ito M, Nakata T, Nishida A, Uetani M,, *Age-related changes in bone density, geometry and biomechanical properties of the proximal femur: CT-based 3D hip structure analysis in normal postmenopausal women.* Bone, 2011. **48**(3): p. 627-630.
49. Maravic M, Ostertag A, Cohen-Solal M, *Subtrochanteric/Femoral Shaft Versus Hip Fractures: Incidences and Identification of Risk Factors.* JBMR, 2011. **27**(1): p. 130-137.
50. Neviaser AS, Lane JM, Lenart BA, Edobor-Osula F, Lorich DG, *Low-energy femoral shaft fractures associated with alendronate use.* J Orthop Trauma, 2008. **22**(5): p. 346-350.
51. Aubrun F, *Hip fracture surgery in the elderly patient: epidemiological data and risk factors.* Ann Fr Anesth Reanim, 2011. **30**(10): p. e37-e39.
52. El Hage R, Moussa E, Jacob C, *Femoral neck geometry in overweight and normal weight adolescent girls.* J Bone Miner Metab, 2010. **28**(5): p. 595-600.
53. El-Kaissi S, Pasco JA, Henry MJ, Panahi S, Nicholson JG, Nicholson GC, Kotowicz MA, *Femoral neck geometry and hip fracture risk: the Geelong osteoporosis study.* Osteoporos Int., 2005. **16**(10): p. 1299-1303.
54. Cheng XG, Lowet G, Boonen S, Nicholson PH, Brys P, Nijs J, Dequeker J, *Assessment of the strength of proximal femur in vitro: relationship to femoral bone mineral density and femoral geometry.* Bone, 1997. **20**(3): p. 213-218.
55. Alonso CG, Curiel MD, Carranza FH, Cano RP, Peréz AD, *Femoral bone mineral density, neck-shaft angle and mean femoral neck width as predictors of hip fracture in men and women. Multicenter Project for Research in Osteoporosis.* Osteoporos Int., 2000. **11**(8): p. 714-720.
56. Center JR, Nguyen TV, Pocock NA, Eisman JA, *Volumetric bone density at the femoral neck as a common measure of hip fracture risk for men and women.* J Clin Endocrinol Metab, 2004. **2004**(89): p. 6.
57. Currey J, *The mechanical adaptations of bones*. 1984, Princeton, NJ.: Princeton University Press.
58. Turner CH, *Bone Strength: Current Concepts.* Ann N Y Acad Sci, 2006.
59. Szulc P, Delmas PD, *Bone loss in elderly men: increased endosteal bone loss and stable periosteal apposition. The prospective MINOS study.* Osteoporos Int., 2007. **18**(4): p. 495-503.

60. Szulc P, Duboeuf F, Schott AM, Dargent-Molina P, Meunier PJ, Delmas PD, *Structural determinants of hip fracture in elderly women: re-analysis of the data from the EPIDOS study.* 17, 2006. **2**(231-236).
61. Kaptoge S, Beck TJ, Reeve J, Stone KL, Hillier TA, Cauley JA, Cummings SR, *Prediction of incident hip fracture risk by femur geometry variables measured by hip structural analysis in the study of osteoporotic fractures.* J Bone Miner Res, 2008. **23**(12): p. 1892-1904.
62. Manske SL, Liu-Ambrose T, de Bakker PM, Liu D, Kontulainen S, Guy P, Oxland TR, McKay HA, *Femoral neck cortical geometry measured with magnetic resonance imaging is associated with proximal femur strength.* Osteoporos Int., 2006. **17**(10): p. 1539-1545.
63. Budynas RG, *Advanced Strength and Applied Stress Analysis*. 2nd ed. 1999: McGraw-Hill Companies.
64. Kim KM, Brown JK, Kim KJ, Choi HS, Kim HN, Rhee Y, Lim SK, *Kim KM, Brown JK, Kim KJ, Choi HS, Kim HN, Rhee Y, Lim SK.* Osteoporos Int., 2011. **22**(7): p. 2165-2174.
65. LaStayo PC, Ewy GA, Pierotti DD, Johns RK, Lindstedt S, *The positive effects of negative work: increased muscle strength and decreased fall risk in a frail elderly population.* J Gerontol A Biol Sci Med Sci, 2003. **58**(5): p. M419-M424.
66. Vicente-Rodriguez G, Ara I, Perez-Gomez J, Dorado C, Calbet JA, *Muscular development and physical activity as major determinants of femoral bone mass acquisition during growth.* Br J Sports Med, 2005. **39**(9): p. 611-616.
67. Högler W, Blimkie CJ, Cowell CT, Inglis D, Rauch F, Kemp AF, Wiebe P, Duncan CS, Farpour-Lambert N, Woodhead HJ, *Sex-specific developmental changes in muscle size and bone geometry at the femoral shaft.* Bone, 2008. **42**(5): p. 982-989.
68. Schoenau E, Neu CM, Mokov E, Wassmer G, Manz F, *Influence of puberty on muscle area and cortical bone area of the forearm in boys and girls.* J Clin Endocrinol Metab, 2000. **85**(3): p. 1095-1098.
69. Schiessl H, Frost HM, Jee WS, *Estrogen and bone-muscle strength and mass relationships.* Bone, 1998. **22**(1): p. 1-6.
70. Travison TG, Araujo AB, Esche GR, Beck TJ, McKinlay JB, *Lean mass and not fat mass is associated with male proximal femur strength.* J Bone Miner Res, 2008. **23**(2): p. 189-198.
71. Dixon WG, Lunt M, Pye SR, Reeve J, Felsenberg D, Silman AJ, O'Neill TW, *Low grip strength is associated with bone mineral density and vertebral fracture in women.* Rheumatology, 2005. **44**(5): p. 643-646.
72. Cipriani C, Romagnoli E, Carnevale V, Raso I, Scarpiello A, Angelozzi M, Tancredi A, Russo S, De Lucia F, Pepe J, Minisola S, *Muscle strength and bone in healthy women: effect of age and gonadal status.* Hormones, 2012. **11**(3): p. 325-332.
73. Marin RV, Pedrosa MA, Moreira-Pfrimer LD, Matsudo SM, Lazaretti-Castro M, *Association between lean mass and handgrip strength with bone mineral density in physically active postmenopausal women.* J Clin Densitom, 2010. **13**(1): p. 96-101.
74. Rutherford OM, Jones DA, *The relationship of muscle and bone loss and activity levels with age in women.* Age Ageing, 1992. **21**(4): p. 286-293.
75. Commean PK, Tuttle LJ, Hastings MK, Strube MJ, Mueller MJ, *Magnetic Resonance Imaging Measurement Reproducibility for Calf Muscle and Adipose Tissue Volume.* J Magn Reson Imaging, 2011. **34**(6): p. 1285-1294.
76. Lang T, Cauley JA, Tylavsky F, Bauer D, Cummings S, Harris TB, *Computed Tomographic Measurements of Thigh Muscle Cross-Sectional Area and Attenuation Coefficient Predict Hip Fracture: The Health, Aging, and Body Composition Study.* J Bone Miner Res, 2010. **25**(3): p. 513-519.
77. Bohannon RW, *Hand-grip dynamometry predicts future outcomes in aging adults.* J Geriatr Phys Ther, 2008. **31**(1): p. 3-10.

78. Nakai R, Azuma T, Sudo M, Urayama S, Takizawa O, Tsutsumi S, *MRI analysis of structural changes in skeletal muscles and surrounding tissues following long-term walking exercise with training equipment.* J Appl Physiol, 2008. **105**(3): p. 958-963.
79. Janz K, *Physical activity and bone development during childhood and adolescence. Implications for the prevention of osteoporosis.* Minerva Pediatr., 2002. **54**(2): p. 93-104.
80. Hansen RD, Williamson DA, Finnegan TP, Lloyd BD, Grady JN, Diamond TH, Smith EU, Stavrinos TM, Thompson MW, Gwinn TH, Allen BJ, Smerdely PI, Diwan AD, Singh NA, Singh MA, *Estimation of thigh muscle cross-sectional area by dual-energy X-ray absorptiometry in frail elderly patients.* Am J Cli Nutr, 2007. **86**(4): p. 952-958.
81. Albanese CV, Diessel E, Genant HK, *Clinical applications of body composition measurements using DXA.* J Clin Densitom, 2003. **6**(2): p. 75-85.
82. Winzenberg T, Jones G, *Dual energy X-ray absorptiometry.* Aust Fam Physician, 2011. **40**(1-2): p. 43-44.
83. Kim J, Wang Z, Heymsfield SB, Baumgartner RN, Gallagher D, *Total-body skeletal muscle mass: estimation by a new dual-energy X-ray absorptiometry method.* Am J Clin Nutr, 2002. **76**(2): p. 378-383.
84. Beck, T., *Measuring the structural strength of bones with dual-energy X-ray absorptiometry: principles, technical limitations, and future possibilities.* Osteoporos Int., 2003. **14**(Suppl 5): p. S81-S88.
85. Beck, T., *Hip Structural Analysis (HSA) Program*. 2002.
86. Bonnick SL, *HSA: beyond BMD with DXA.* Bone, 2007. **41**(1 Suppl 1): p. S9-S12.
87. Adams JE, *Quantitative computed tomography.* Eur J Radiol, 2009. **71**(3): p. 415-424.
88. Johnston JD, Masri BA, Wilson DR, *Computed tomography topographic mapping of subchondral density (CT-TOMASD) in osteoarthritic and normal knees: methodological development and preliminary findings.* Osteoarthritis Cartilage, 2009. **17**(10): p. 1319-1326.
89. Kalender WA, *CT: the unexpected evolution of an imaging modality.* Eur Radiol, 2005. **15**(Suppl 4): p. D21-D24.
90. Ito M, Wakao N, Hida T, Matsui Y, Abe Y, Aoyagi K, Uetani M, Harada A, *Analysis of hip geometry by clinical CT for the assessment of hip fracture risk in elderly Japanese women.* Bone, 2010. **46**(2): p. 452-457.
91. Ito M, *Recent progress in bone imaging for osteoporosis research.* J Bone Miner Metab, 2011. **29**(2): p. 131-140.
92. Jordan R, Dickenson E, Westacott D, Baraza N, Srinivasan K, *A vast increase in the use of CT scans for investigating occult hip fractures.* Eur J Radiol, 2013.
93. Kang Y, Engelke K, Kalender WA, *A new accurate and precise 3-D segmentation method for skeletal structures in volumetric CT data.* IEEE Trans Med Imaging, 2003. **22**(5): p. 586-598.
94. Stiehl JB, Jacobson D, Carrera G, *Morphological analysis of the proximal femur using quantitative computed tomography.* Int Orthop, 2007. **31**(3): p. 287-292.
95. Lang TF, Keyak JH, Heitz MW, Augat P, Lu Y, Mathur A, Genant HK, *Volumetric quantitative computed tomography of the proximal femur: precision and relation to bone strength.* Bone, 1997. **21**(1): p. 101-108.
96. Lang T, Koyama A, Li C, Li J, Lu Y, Saeed I, Gazze E, Keyak J, Harris T, Cheng X, *Pelvic body composition measurements by quantitative computed tomography: Association with recent hip fracture.* Bone, 2008. **42**(4): p. 798-805.
97. Fred HL, *Drawbacks and Limitations of Computed Tomography.* Tex Heart Inst J, 2004. **31**(4): p. 345-348.
98. Engelke K, *Assessment of bone quality and strength with new technologies.* Curr Opin Endocrinol Diabetes Obes, 2012. **19**(6): p. 474-482.
99. Engelke K, Adams JE, Armbrecht G, Augat P, Bogado CE, Bouxsein ML, Felsenberg D, Ito M, Prevrhal S, Hans DB, Lewiecki EM, *Clinical use of quantitative computed tomography and*

peripheral quantitative computed tomography in the management of osteoporosis in adults: the 2007 ISCD Official Positions. J Clin Densitom, 2008. **11**(1): p. 123-162.
100. Damilakis J, Adams JE, Guglielmi G, Link TM., *Radiation exposure in X-ray-based imaging techniques used in osteoporosis.* Eur Radiol, 2010. **20**(11): p. 2707-2714.
101. Canadian Nuclear Safety Commission, *Radiation Doses - Sources and Average Effective Dose from Natural Background Radiation in Selected Canadian Cities*. 2013.
102. UNSCEAR, *Report to the General Assembly e Annex B: Exposures from Natural Radiation Sources. Sources and Effects of Ionizing Radiation. United Nations Scientific Committee on the Effects of Atomic Radiation*. 2000.
103. Westbrook C, Roth CK, Talbot J, *MRI in practice*. 4th ed. 2011.
104. Hendee WR, Morgan CJ, *Magnetic Resonance Imaging Part I - Physical Principles.* West J Med, 1984. **141**: p. 491-500.
105. Gomberg BR, Saha PK, Wehrli FW, *Method for Cortical Bone Structural Analysis from Magnetic Resonance Images.* Acad Radiol, 2005. **12**(10): p. 1320-1332.
106. McKay HA, Sievänen H, Petit MA, MacKelvie KJ, Forkheim KM, Whittall KP, Forster BB, Macdonald H, *Application of magnetic resonance imaging to evaluation of femoral neck structure in growing girls.* J Clin Densitom, 2004. **7**(2): p. 161-168.
107. Majumdar S, *A review of magnetic resonance (MR) imaging of trabecular bone micro-architecture: contribution to the prediction of biomechanical properties and fracture prevalence.* Technol Health Care, 1998. **6**(5-6): p. 321-327.
108. Krug R, Banerjee S, Han ET, Newitt DC, Link TM, Majumdar S, *Feasibility of in vivo structural analysis of hihg-resolution magnetic resonance images of the proximal femur.* Osteoporos Int., 2005. **16**(11): p. 1307-1314.
109. Woodhead HJ, Kemp AF, Blimkie CJR, Briody JN, Duncan CS, Thompson M, Lam A, Howman-Giles R, Cowell CT, *Measurement of Midfemoral Shaft Geometry: Repeatability and Accuracy Using Magnetic Resonance Imaging and Dual-Energy X-ray Absorptiometry.* J Bone Miner Res, 2001. **16**(12): p. 2251-2259.
110. Glüer CC, Blake G, Lu Y, Blunt BA, Jergas M, Genant HK, *Accurate assessment of precision errors: how to measure the reproducibility of bone densitometry techniques.* Osteoporos Int. , 1995. **5**(4): p. 262-270.
111. Pan J, *Image Interpolation using Spline Curves.* 2003.
112. Ito M, Nakamura T, Fukunaga M, Shiraki M, Matsumoto T, *Effect of eldecalcitol, an active vitamin D analog, on hip structure and biomechanical properties: 3D assessment by clinical CT.* Bone, 2011. **49**(3): p. 328-334.
113. Fajardo RJ, Ryan TM, Kappelman J, *Assessing the accuracy of high-resolution X-ray computed tomography of primate trabecular bone by comparisons with histological sections.* American Journal of Physical Anthropology, 2002. **118**(1): p. 1-10.
114. Spoor CF, Zonneveld FW, Macho GA, *Linear measurements of cortical bone and dental enamel by computed tomography: applications and problems.* American Journal of Physical Anthropology, 1993. **91**(4): p. 469-484.
115. Nelson L, Gulenchyn KY, Atthey M, Webber CE, *Is a fixed value for the least significant change appropriate?* J Clin Densitom, 2010. **13**(1): p. 18-23.
116. Wu HT, Chang CY, Chang H, Yen CC, Cheng H, Chen PC, Chiou HJ, *Magnetic resonance imaging guided biopsy of musculoskeletal lesions.* J Chin Med Assoc, 2012. **75**(4): p. 160-166.
117. Khoo BC, Beck TJ, Qiao QH, Parakh P, Semanick L, Prince RL, Singer KP, Price RI, *In vivo short-term precision of hip structure analysis variables in comparison with bone mineral density using paired dual-energy X-ray absorptiometry scans from multi-center clinical trials.* Bone, 2005. **37**(1): p. 112-121.
118. Tuck SP, Rawlings DJ, Scane AC, Pande I, Summers GD, Woolf AD, Francis RM, *Femoral neck shaft angle in men with fragility fractures.* J Osteoporos, 2011.

119. Forsberg AM, Nilsson E, Werneman J, Bergstrom J, Hultman E, *Muscle composition in relation to age and sex*. Clin Sci (Lond), 1991. **81**(2): p. 249-256.
120. Goodpaster BH, Kelley DE, Thaete FL, He J, Ross R, *Skeletal muscle attenuation determined by computed tomography is associated with skeletal muscle lipid content.* J Appl Physiol, 2000. **89**(1): p. 104-110.
121. Song MY, Ruts E, Kim J, Janumala I, Heymsfield, Gallagher D, *Sarcopenia and increased adipose tissue infiltration of muscle in elderly African American women.* Am J Clin Nutr, 2004. **79**(5): p. 874-880.
122. Harris T, *Muscle mass and strength: relation to function in population studies.* J Nutr, 1997. **127**(5 Suppl): p. 1004S-1006S.